THE ASTROPHYSICAL JOURNAL SUPPLEMENT SERIES, 60:297–303, 1986 January

MASSACHUSETTS–STONY BROOK GALACTIC PLANE CO SURVEY. II. (l, V) MAPS OF THE FIRST GALACTIC QUADRANT

D. P. CLEMENS AND D. B. SANDERS
Five College Radio Astronomy Observatory; and Department of Physics and Astronomy, University of Massachusetts, Amherst
N. Z. SCOVILLE
Five College Radio Astronomy Observatory; Department of Physics and Astronomy, University of Massachusetts, Amherst; and Department of Astronomy, California Institute of Technology
AND
P. M. SOLOMON
Astronomy Program, State University of New York at Stony Brook
Received 1984 November 19; accepted 1985 June 5

ABSTRACT

The Massachusetts–Stony Brook Galactic Plane CO Survey data set, consisting of 40,551 ^{12}CO $J=1$–0 spectra covering longitudes 8°–90° and latitudes −1°.05 to +1°, is presented in longitude-velocity (l, V) format. Spectra from the 42 latitudes sampled were averaged to yield seven (l, V) gray scale maps with 18′ latitude resolution. One contour (l, V) map along the Galactic equator is included to show the spatially clumpy nature of the CO emission. The integrated CO intensity is presented as a function of longitude for the 18′ averaged data, and as a function of longitude and latitude in contour and gray scale maps at the full survey spatial resolution. The presentations of the data set contained here are most useful for comparison with other Galactic surveys of the first quadrant, for tracing out large-scale features, and for identifying emission-line velocities associated with continuum (e.g., radio and *IRAS*) sources.

Subject headings: galaxies: Milky Way — galaxies: structure — interstellar: molecules

I. INTRODUCTION

This is the second paper in a series which presents the data and results derived from the Massachusetts–Stony Brook Galactic Plane CO Survey. A full discussion of the survey data collection method, calibration, and coverage is contained in the first paper (Sanders *et al.* 1986, hereafter Paper I). This survey is the most comprehensive study of Galactic molecular clouds performed to date. The more than 40,000 spectra obtained on a (mostly) 3′ spatial grid using a 45″ beamwidth offer a unique opportunity to resolve the Galactic emission into its constituent molecular clouds. In addition, the large longitude coverage enables the tracing-out of large-scale features and the probing of the spiral structure of the Galaxy.

Paper I presented the data set as 1190 separate latitude-velocity (b, V) contour maps. This format is useful for distinguishing individual molecular clouds and examining the Z-dependence of molecular emission. Paper III (Solomon *et al.* 1986) will present the data as spatial (l, b) maps at constant velocity, which facilitates the identification of clouds, cloud complexes, and warps of the Galactic plane. A later paper will present, in tabular form, the catalog of the individual molecular clouds identified within the data set.

In this paper the data are presented in longitude-velocity (l, V) format. This method of display is useful for studying large-scale Galactic features, such as spiral arms or segments, as well as enabling direct comparison with Galactic emission distributions of other surveys (recombination line, radio continuum, infrared, and so on). In addition, individual sources present in continuum surveys (e.g., radio, *IRAS*), taken with similar spatial resolution, may have their associated emission velocities determined by consulting the (l, V) maps.

The following section presents the (l, V) gray scale and $b=0°$ contour maps followed by plots of the integrated CO emission as a function of longitude for each latitude range. Contour and gray scale maps are then presented to show the integrated CO emission versus Galactic longitude and latitude.

II. LONGITUDE-VELOCITY MAPS

Parameters relevant to the present maps are as follows. The 40,551 CO $J=1$–0 spectra are distributed over 1190 longitudes and 42 latitudes. From $l=18°$ to $l=55°$ (sufficient to cover almost all of the Galactic molecular ring), the Galactic plane was sampled on a 3′×3′ grid from $b=-1°.05$ to $b=+1°.00$. Over the regions $l=8°$–17°.9 and 55°.1–89°.9 from $b=-1°$ to $b=+1°$, the plane was sampled on a 6′×6′ grid.

The beamwidth of the 14 m Five College Radio Astronomy Observatory[1] (FCRAO) telescope was 45″ (FWHM) at 2.6 mm wavelength. In the reduced data, the spectral coverage of 301 km s^{-1} (usually covering $V_{LSR}=-100$ to +200 km s^{-1}) is presented at 1 km s^{-1} resolution. The data are in T_R^* units, and the mean baseline noise level is 0.4 K.

[1]The Five College Radio Astronomy Observatory is operated with support from the National Science Foundation under grant AST 82-12252, and with the permission of the Metropolitan District Commission, Commonwealth of Massachusetts.

Spectra from the 42 latitudes sampled were averaged to form seven longitude-velocity maps (Figs. 1*a*–1*g* [Pls. 1–7]). Because the molecular clouds have a scale height of about 120 pc (FWHM), the samples at larger latitudes tend to be preferentially populated with nearby material. The more central latitudes will sample clouds throughout the Galactic disk. Each map is characterized by a latitude resolution of 18′ and longitude resolution of 3′ and 6′ (see previous section). The latitude range covered by each map is indicated in the upper right-hand corner of the map. The velocity resolution is 1 km s^{-1}. The display of data in each map was truncated below 1 K (4 or 6 times the rms baseline noise, depending on the sample grid) and the gray scale saturated at 3 K, as shown in the inset gray scale "wedge" on Figure 1*d*.

The principal characteristics of the CO emission seen in Figure 1 are as follows:

1. Much of the emission is concentrated into the region bounded by $l = 20°$ and $l = 50°$ and $V_{LSR} > 20$ km s^{-1}. This region corresponds to the molecular cloud ring found by Scoville and Solomon (1975) for Galactic radii between 4 and 8 kpc. The strong emission along the high-velocity edge ($V = 90$–120 km s^{-1}) between $l = 23°$ and $l = 32°$ originates from the peak of the ring at 5–5.5 kpc radius.

2. Very little emission occurs at negative velocities and at longitudes greater than 52°. The former corresponds to the region of the Galaxy outside the solar circle, and the latter to radii greater than 8 kpc. Solomon, Stark, and Sanders (1983) found some emission at $b \sim 1\overset{\circ}{.}5$ for $R = 1.3$–$1.5\ R_\odot$, but conclude that less than 10% of the Galactic CO emission is beyond the solar circle.

3. There are large-scale features present. Some, especially those near zero velocity, and present in the highest $|b|$ maps, are due to the large angular extent of nearby giant molecular clouds such as W44 at $l \sim 35°$ and M17 at $l \sim 15°$. Others, such as the one extending from $l = 9°$, $V_{LSR} = -20$ km s^{-1}, to $l = 14°$, $V_{LSR} = +20$ km s^{-1}, on the $b = -0\overset{\circ}{.}45$ to $-0\overset{\circ}{.}20$ map (the "3 kpc arm"; Rougoor and Oort 1960) are truly Galactic features, containing many massive molecular clouds. Another Galactic feature at 7.5 kpc radius is evident between $l = 34°$ and $l = 50°$ ($V = 50$–65 km s^{-1}) in the $b = -0\overset{\circ}{.}45$ to $-0\overset{\circ}{.}20$ map. There are also pronounced minima in the (l, V)-plane in the 18′ maps (see also Cohen *et al.* 1980), such as the region between $l = 24°$ and $l = 27°$ and $V = 70$–80 km s^{-1}. When examined at 3′ resolution, these regions show significant CO emission from lower intensity clouds (Solomon, Sanders, and Rivolo 1985).

4. The Galactic disk is warped in the inner Galaxy (Cohen and Thaddeus 1977; Sanders, Solomon, and Scoville 1984). Note, for example, the maps for $b = -1\overset{\circ}{.}05$ to $-0\overset{\circ}{.}80$ (Fig. 1*g*) and $b = +0\overset{\circ}{.}45$ to $+0\overset{\circ}{.}70$ (Fig. 1*b*). The former is dominated by emission from $l = 8°$, $V_{LSR} = 15$ km s^{-1}, to $l = 30°$, $V_{LSR} = 70$–80 km s^{-1}, while the latter map shows no corresponding emission. Instead, the second map shows a strong concentration of clouds at $l = 23°$, $V_{LSR} = 90$ km s^{-1}, which are entirely absent in the first map.

The gray scale figures, because they are 18′ averages in latitude, tend to represent poorly the clumpy and cloudlike appearance of the data. Figure 2 (Plates 8–10) is a contour map of $b = 0°$ data only; it is better able to show individual molecular clouds. The lowest contour is at 1.25 K (3 σ), and subsequent contours are at integer temperatures (2,3,4,...). The longitudes sampled are indicated by tick marks along the vertical axes. Smooth features in the gray scale (l, V) diagrams break up into a myriad of individual molecular clouds in the figure. For example, analysis of an (l, V) contour map at $b = 0°$ between $l = 23°$ and $l = 30°$ led to the finding that most of the CO emission in the Galaxy came from giant molecular clouds (Solomon, Sanders, and Scoville 1979), objects with sizes of 20–80 pc.

III. INTEGRATED CO EMISSION

The integrated CO intensity along each (l, b) line of sight is related to the amount of molecular material present in the telescope beam.[2] For comparison of the molecular column density with other tracers of interstellar gas, Figures 3*a*–3*g* show $\langle \int T_R^*(\mathrm{CO})\, dV \rangle$, in K km s^{-1}, for velocities between -50 and 160 km s^{-1}, as a function of longitude for each latitude range. The noise level in the plots is about 10 K km s^{-1}; 6 K km s^{-1} arises from individual channel baseline noise, and some small contribution from baseline curvature is undoubtedly present.

Figure 3 is most useful for comparing CO intensities with continuum observations; e.g., the recent FIR data of Caux *et al.* (1984) shows excellent correspondence with the strongest features in Figure 3*d* at longitudes 13°, 24°, 31°, and 49° while disagreeing at 83°. While Figure 3 is similar to the CO integrated intensity diagram shown by Robinson *et al.* (1984), the current plots differ by possessing much higher longitudinal resolution and by displaying the CO intensity away from the Galactic equator.

A final presentation of the data is given in Figures 4–20 (Plates 11–27).[3] These maps show in contour (Figs. 4–20, *upper panels*) and gray scale (Figs. 4–20, *lower panels*) formats the distribution of integrated CO emission with Galactic longitude and latitude. The contours in the upper panels begin at 30 K km s^{-1} and are stepped by 30 K km s^{-1}. The lower panels are provided to resolve ambiguities in contour gradients and to give a visual impression of the molecular Galactic plane. A gray scale "wedge" is shown on Figure 4, indicating a lower cutoff of 30 K km s^{-1} and saturation at 240 K km s^{-1}.

The molecular ring is visible in the figures, as strong emission from 20° to 40° longitude, as are warps of the molecular disk away from the Galactic equator. The emission drops strongly with increasing longitude beyond $l = 52°$ and is quite weak and patchy out to $l = 90°$, with the exception of the moderately strong Cygnus region from $l \sim 74°$ to $l = 81°$.

A project of this size and scope is accomplished only by the efforts of a large number of talented people. The smooth and efficient operation of the 14 m telescope derives directly from the care and expertise of the FCRAO staff, scientists, and

[2] The value of the constant used to derive the equivalent hydrogen column density has been found by Sanders, Solomon, and Scoville (1984) to be 3.6×10^{20} H_2 cm^{-2} (K km $s^{-1})^{-1}$ and determined from γ-ray (*COS B*) and CO observations to be $(2.6 \pm 1.2) \times 10^{20}$ H_2 cm^{-2} (K km $s^{-1})^{-1}$ by Bloemen *et al.* (1984).

[3] Color slides of Figs. 4–20 are available from the authors at cost.

FIG. 3.—Plots of the integrated CO intensity, $\int T_R^*(\mathrm{CO})\, dV$, for velocities between -50 and $+160$ km s^{-1}, versus longitude for the indicated latitude intervals. The longitudinal resolution is 3′ between $l = 18°$ and $l = 55°$, and 6′ elsewhere. The noise level (1 σ) is about 10 K km s^{-1}. (*a*) From $b = +0\overset{\circ}{.}75$ to $b = +1\overset{\circ}{.}00$. (*b*) from $b = +0\overset{\circ}{.}45$ to $b = +0\overset{\circ}{.}70$. (*c*) From $b = +0\overset{\circ}{.}15$ to $b = +0\overset{\circ}{.}40$. (*d*) From $b = -0\overset{\circ}{.}15$ to $b = +0\overset{\circ}{.}10$. (*e*) From $b = -0\overset{\circ}{.}45$ to $b = -0\overset{\circ}{.}20$. (*f*) From $b = -0\overset{\circ}{.}50$ to $b = -0\overset{\circ}{.}75$. (*b*) From $b = -1\overset{\circ}{.}05$ to $b = -0\overset{\circ}{.}80$.

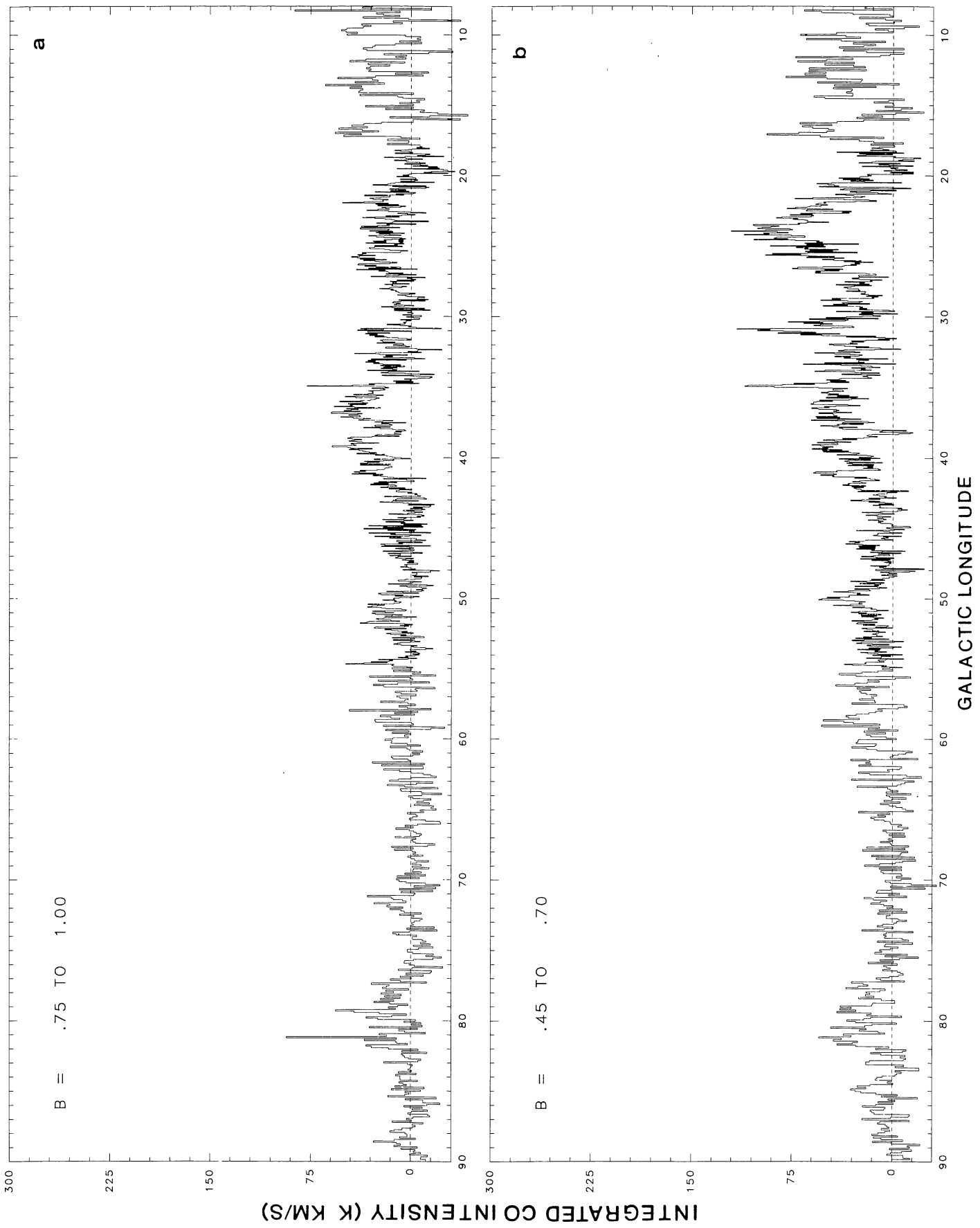

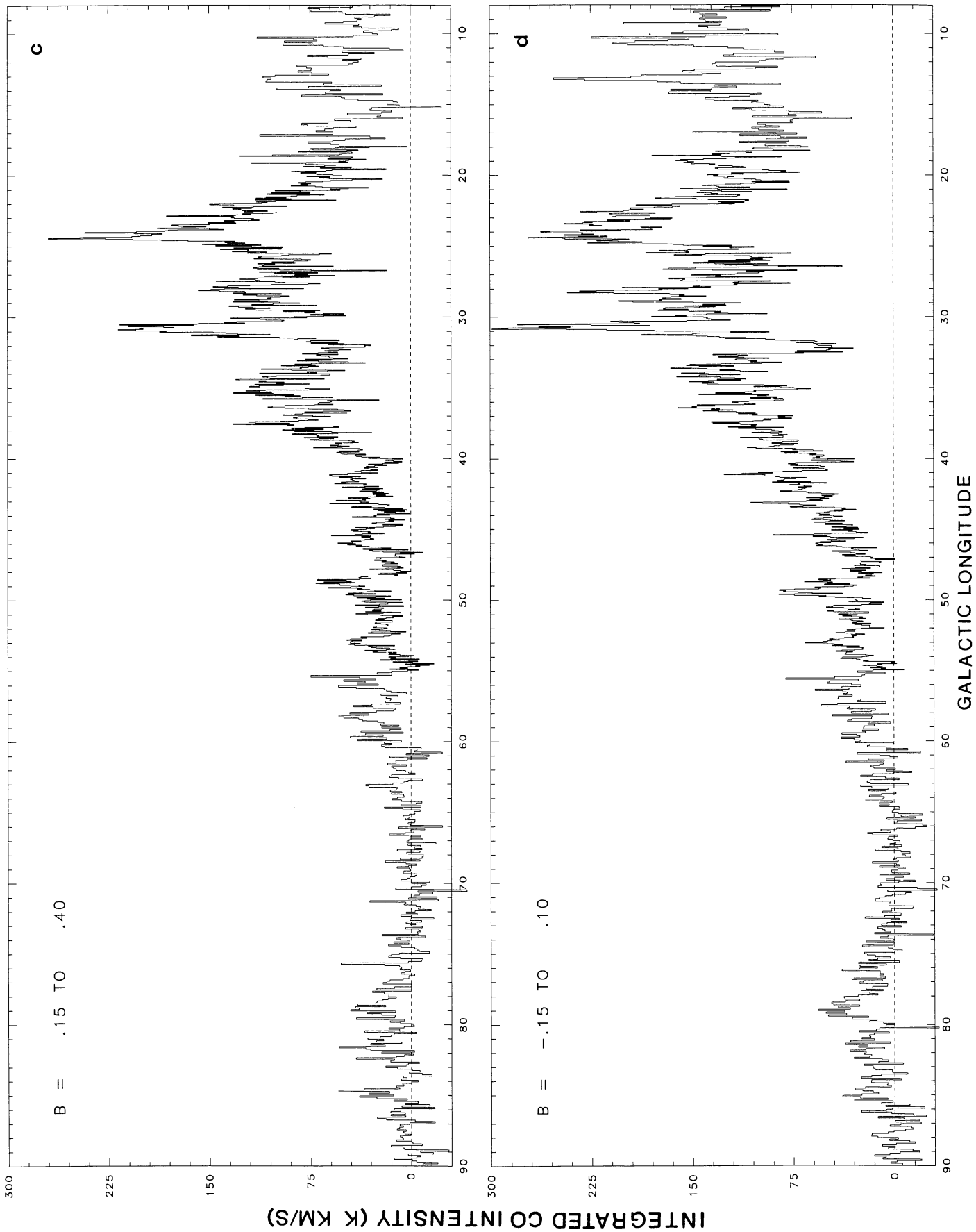

FIG. 3—*Continued*

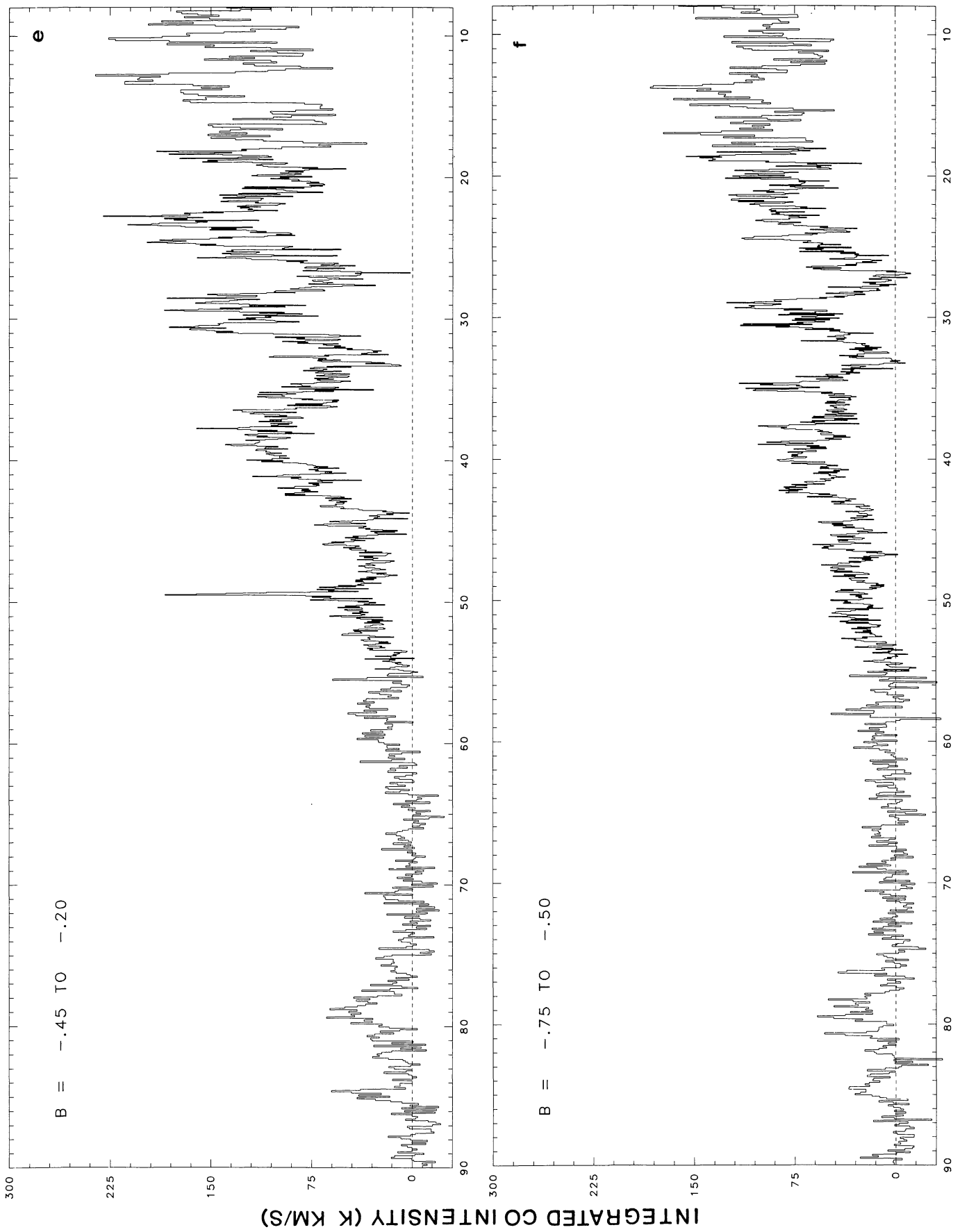

FIG. 3—*Continued*

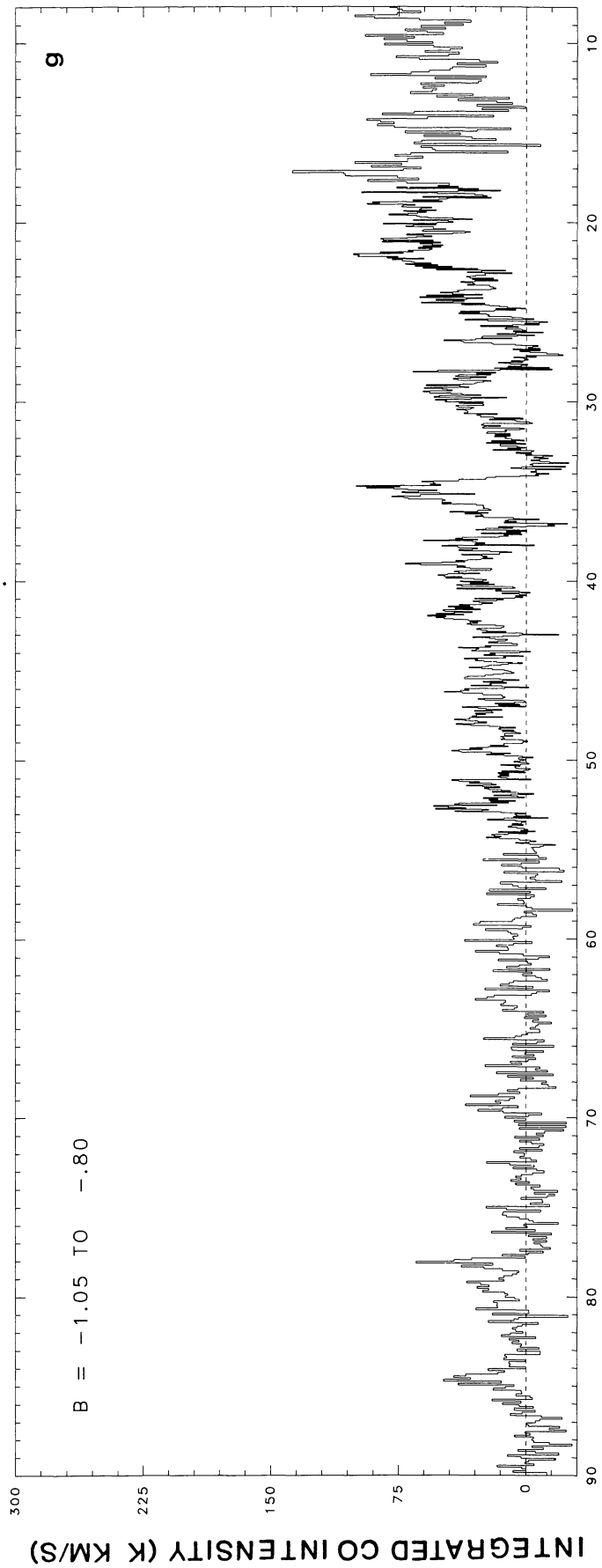

FIG. 3—*Continued*

students. Data management, analysis, and display have utilized the excellent resources of the University of Massachusetts Computer Center on the Amherst campus. Individuals requiring special thanks include Duncan Chesley, Rick Newton, John Good, Bill Waller, and Peter deFriesse. Figures 1 and 4–20 were prepared on a RAMTEK 9400 color graphics display and written to film using an OPTRONICS C4500 digital photowriter, both operated by the Digital Image Analysis Laboratory, University of Massachusetts at Amherst. This is Contribution No. 588 of the Five College Astronomy Department.

REFERENCES

Bloemen, J. B. G. M., Carraveo, P. A., Hermsen, W., Lebrun, F., Maddalena, R. J., Strong, A. W., and Thaddeus, P. 1984, *Astr. Ap.*, **139**, 37.
Caux, E., Serra, G., Gispert, R., Puget, J. L., Ryter, C., and Coron, N. 1984, *Astr. Ap.*, **137**, 1.
Cohen, R. S., Cong, H., Dame, T. M., and Thaddeus, P. 1980, *Ap. J. (Letters)*, **239**, L53.
Cohen, R. S., and Thaddeus, P. 1977, *Ap. J. (Letters)*, **207**, L189.
Reich, W., Fuerst, E., Steffen, P., Reif, K., and Haslam, C. G. T. 1984, *Astr. Ap. Suppl.*, **58**, 197.
Robinson, B. J., Manchester, R. N., Whiteoak, J. B., Sanders, D. B., Scoville, N. Z., Clemens, D. P., and Solomon, P. M. 1984, *Ap. J. (Letters)*, **283**, L31.
Rougoor, G. W., and Oort, J. H. 1960, *Proc. Nat. Acad. Sci.*, **46**, 1.
Sanders, D. B., Clemens, D. P., Scoville, N. Z., and Solomon, P. M. 1986, *Ap. J. (Suppl.)*, **60**, 1 (Paper I).
Sanders, D. B., Solomon, P. M., and Scoville, N. Z. 1984, *Ap. J.*, **276**, 182.
Scoville, N. Z., and Solomon, P. M. 1975, *Ap. J. (Letters)*, **199**, L105.
Solomon, P. M., Sanders, D. B., Clemens, D. P., and Scoville, N. Z. 1986, *Ap. J. (Suppl.)*, in preparation (Paper III).
Solomon, P. M., Sanders, D. B., and Rivolo, A. R. 1985, *Ap. J. (Letters)*, **292**, L19.
Solomon, P. M., Sanders, D. B., and Scoville, N. Z. 1979, in *IAU Symposium 84, The Large-Scale Characteristics of the Galaxy*, ed. W. B. Burton (Dordrecht: Reidel), p. 35.
Solomon, P. M., Stark, A. A., and Sanders, D. B. 1983, *Ap. J. (Letters)*, **267**, L29.

D. P. Clemens: Steward Observatory, University of Arizona, Tucson, AZ 85721

D. B. Sanders: Downs Laboratory, 320-47, California Institute of Technology, Pasadena, CA 91125

N. Z. Scoville: Department of Astronomy, 105-24, California Institute of Technology, Pasadena, CA 91125

P. M. Solomon: Astrophysics Program, Department of Earth and Space Sciences, State University of New York, Stony Brook, NY 11794

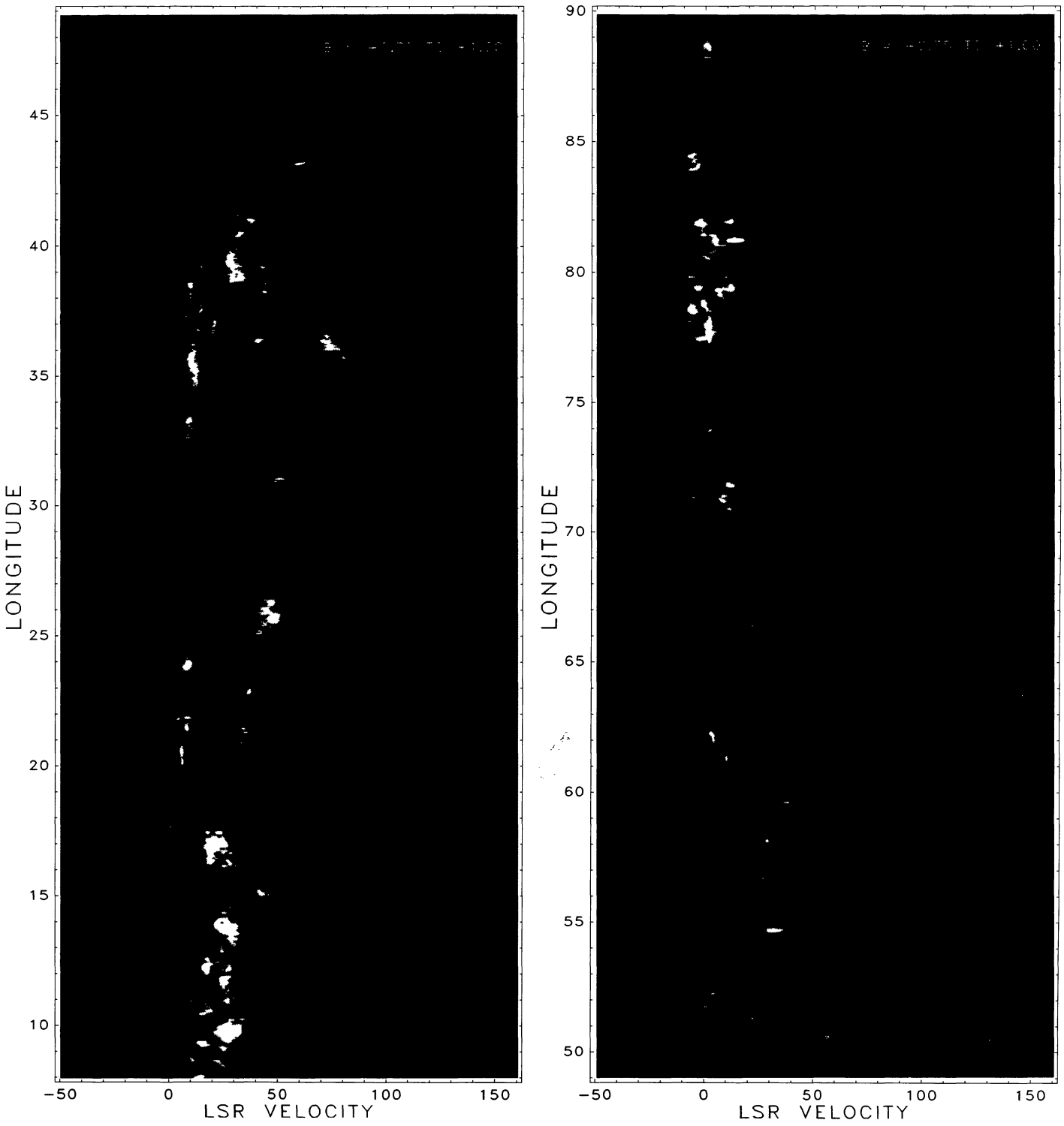

FIG. 1*a*

FIG. 1.—Longitude-velocity (l, V) gray scale map for the indicated latitudes. Longitudinal resolution is 3′ between $l = 18°$ and $l = 55°$, and 6′ elsewhere. Velocity resolution is 1 km s^{-1}. Calibration scale is shown in Fig. 1*d*. *Left-hand panel*: $l = 8°$–$49°$. *Right-hand panel*: $l = 49°$–$90°$. (*a*) Latitudes between +0°.75 and +1°.00. (*b*) Latitudes between +0°.45 and +0°.70. (*c*) Latitudes between +0°.15 and +0°.40. (*d*) Latitudes between −0°.15 and +0°.10. Gray scale "wedge" indicates the conversion from gray level to corrected radiation temperature, T_R^*. Lower cutoff is at 1.0 K, and saturation is at 3 K. (*e*) Latitudes between −0°.45 and −0°.20. (*f*) Latitudes between −0°.75 and −0°.50. (*g*) Latitudes between −1°.05 and −0°.80.

PLATE 2

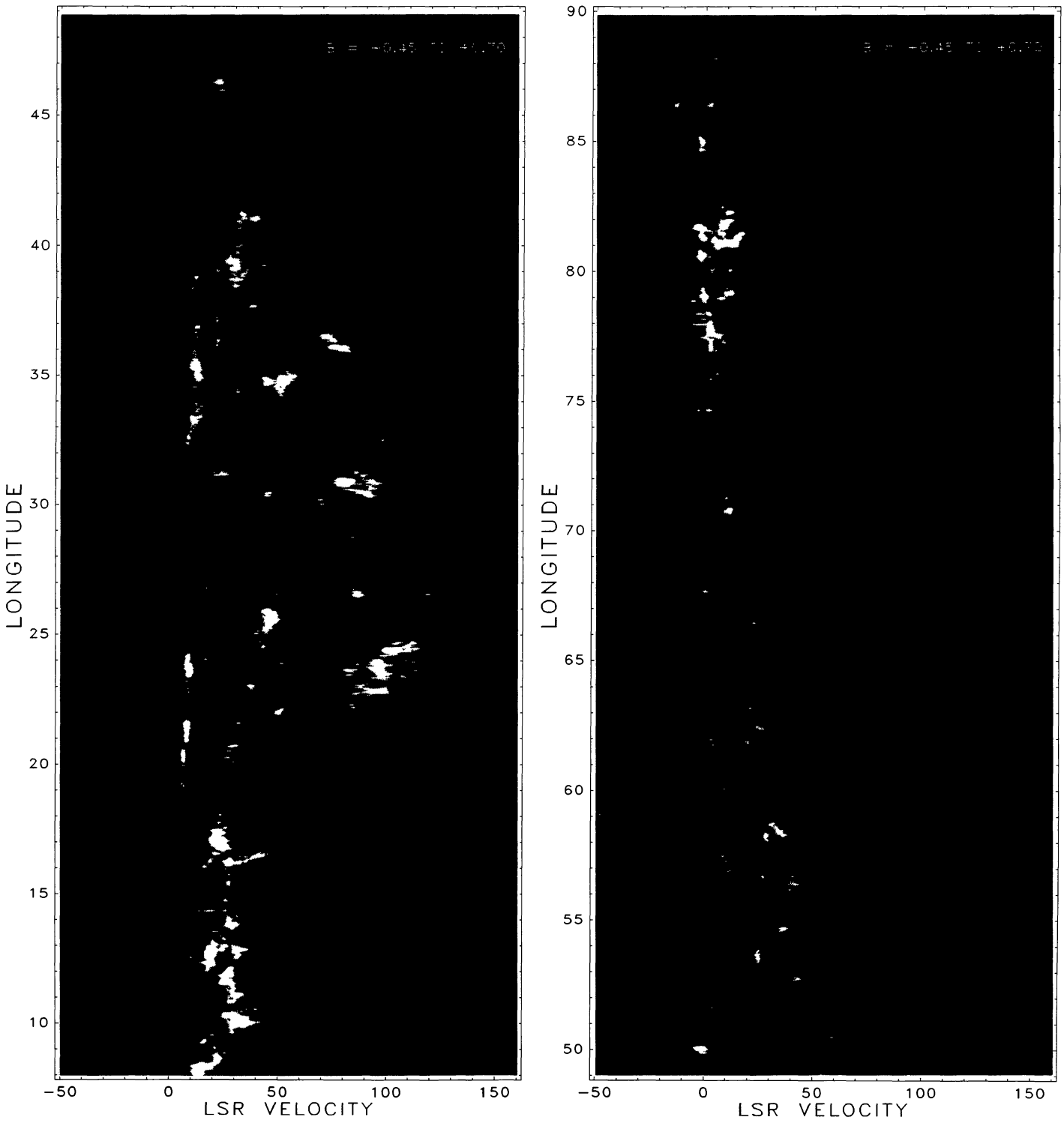

FIG. 1*b*

CLEMENS, SANDERS, SCOVILLE, AND SOLOMON (*see* page 298)

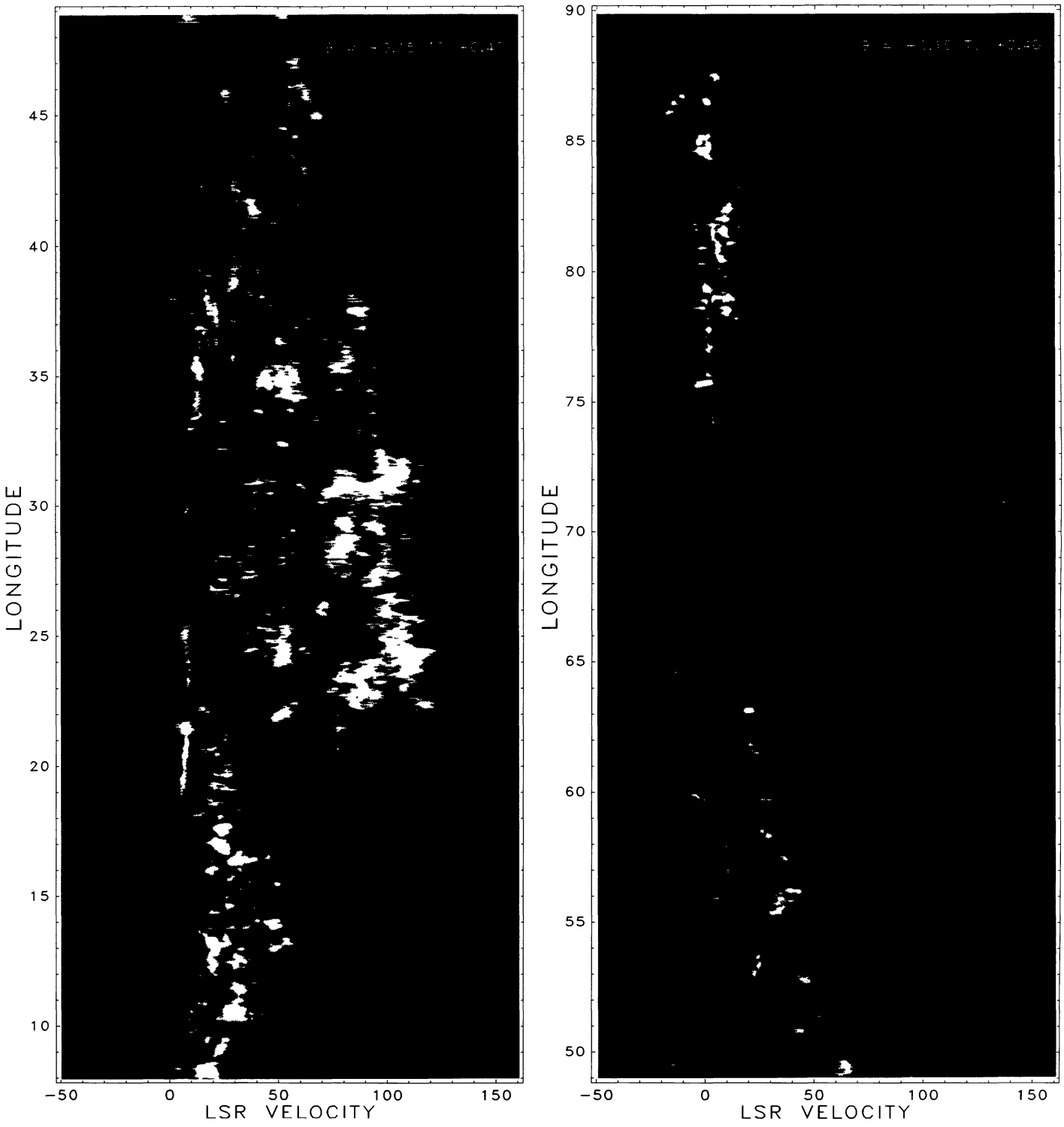

FIG. 1*c*

CLEMENS, SANDERS, SCOVILLE, AND SOLOMON (*see* page 298)

PLATE 4

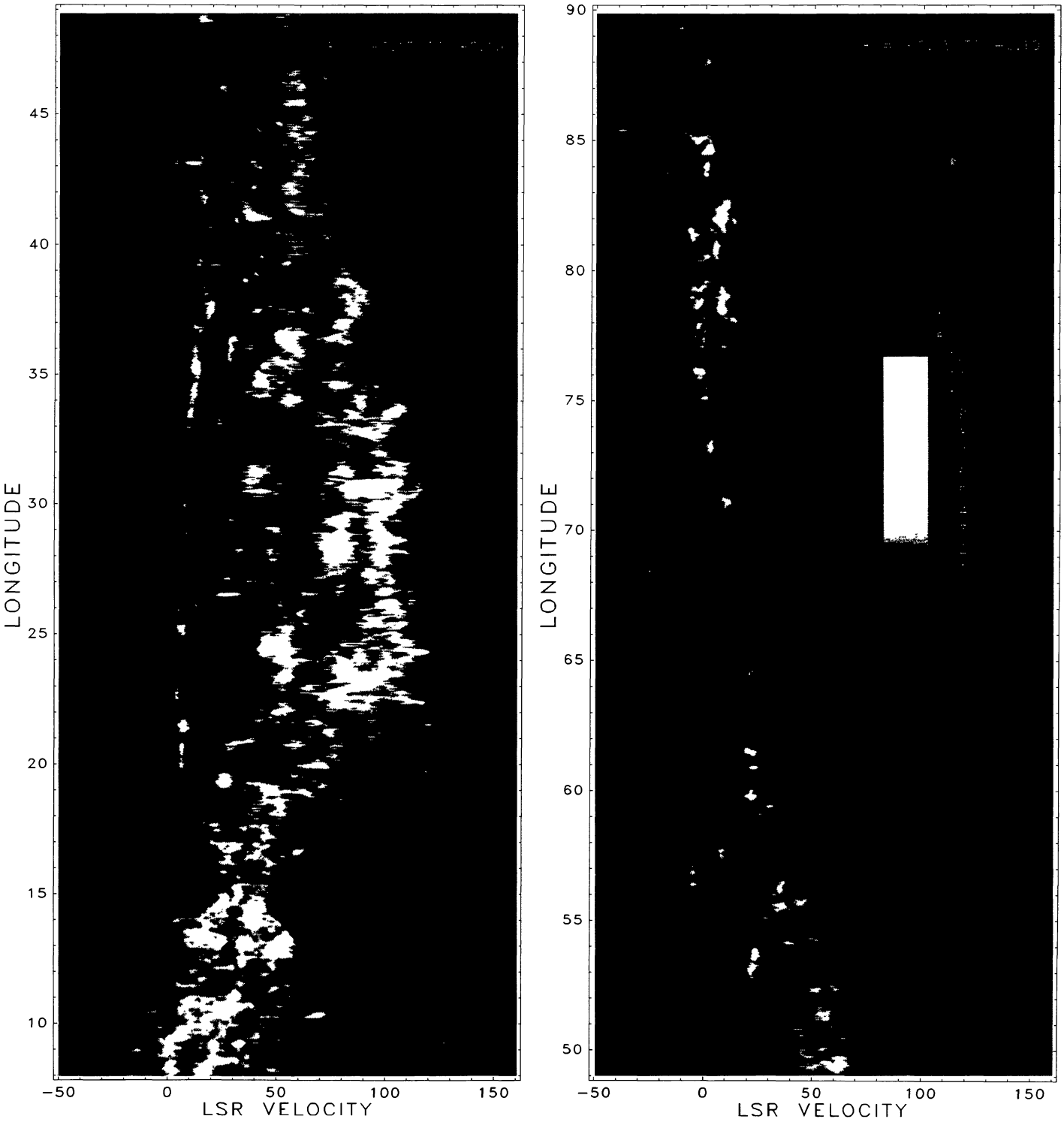

FIG. 1*d*

CLEMENS, SANDERS, SCOVILLE, AND SOLOMON (*see* page 298)

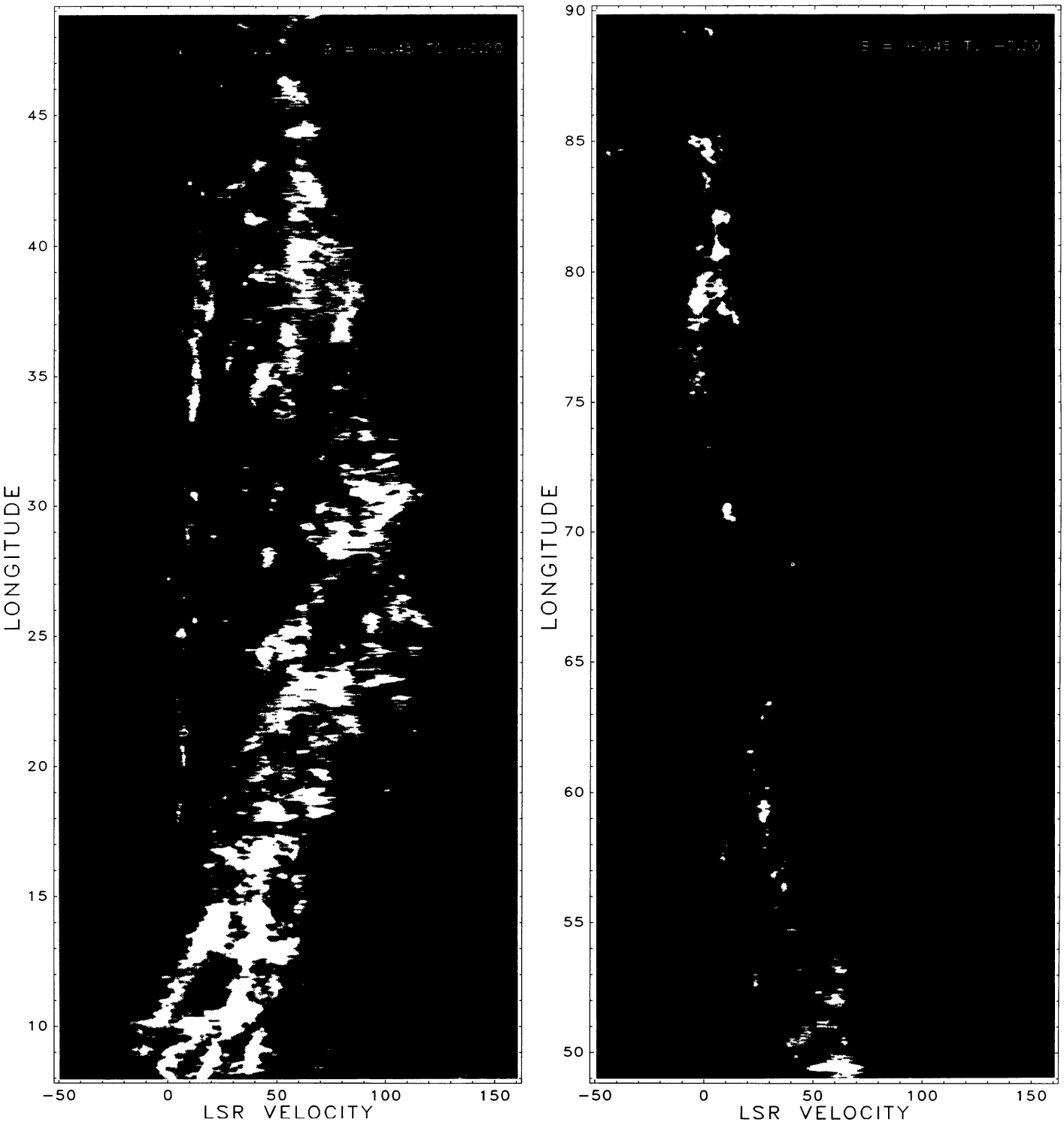

FIG. 1*e*

CLEMENS, SANDERS, SCOVILLE, AND SOLOMON (*see* page 298)

PLATE 6

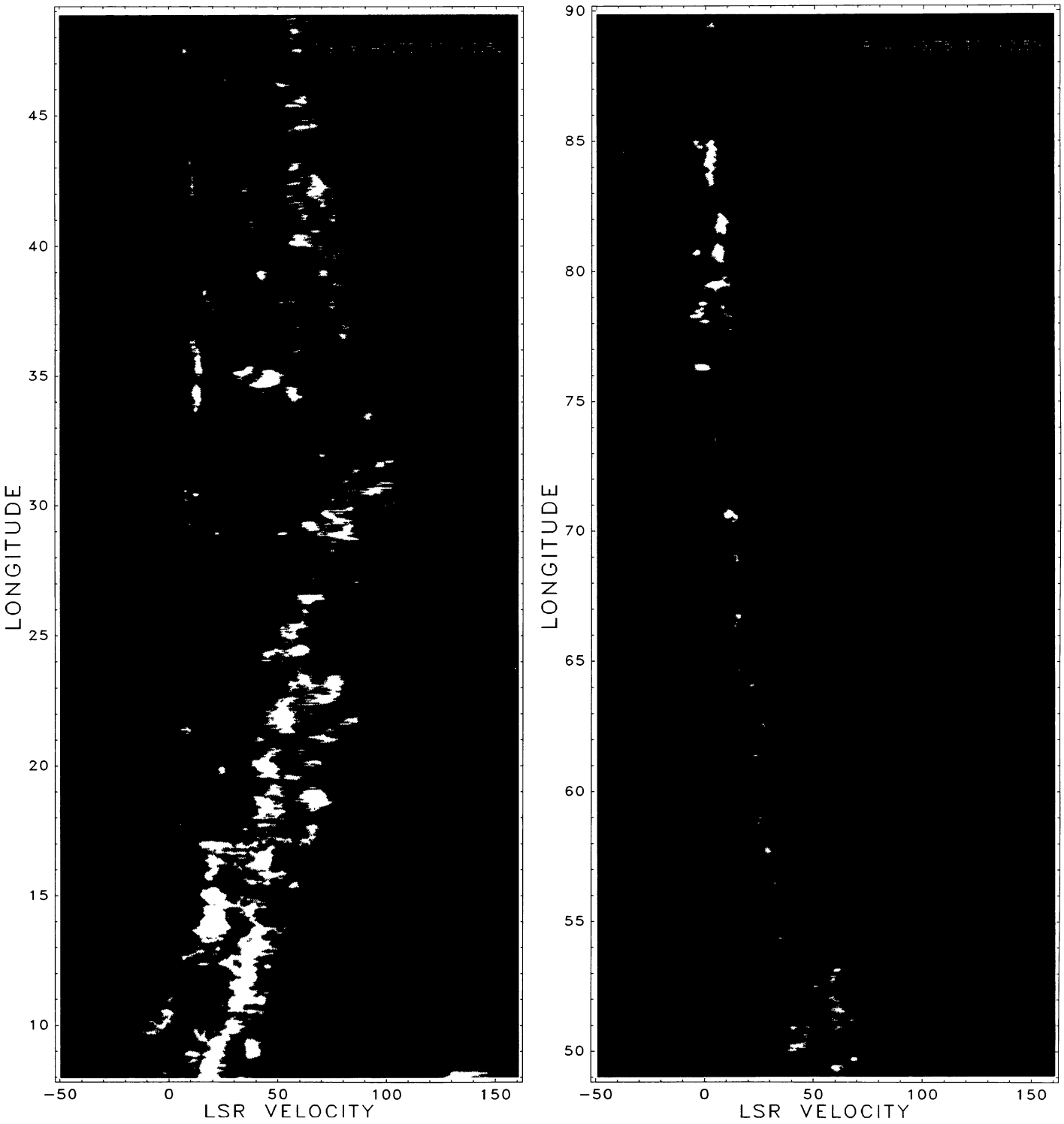

FIG. 1*f*

CLEMENS, SANDERS, SCOVILLE, AND SOLOMON (*see* page 298)

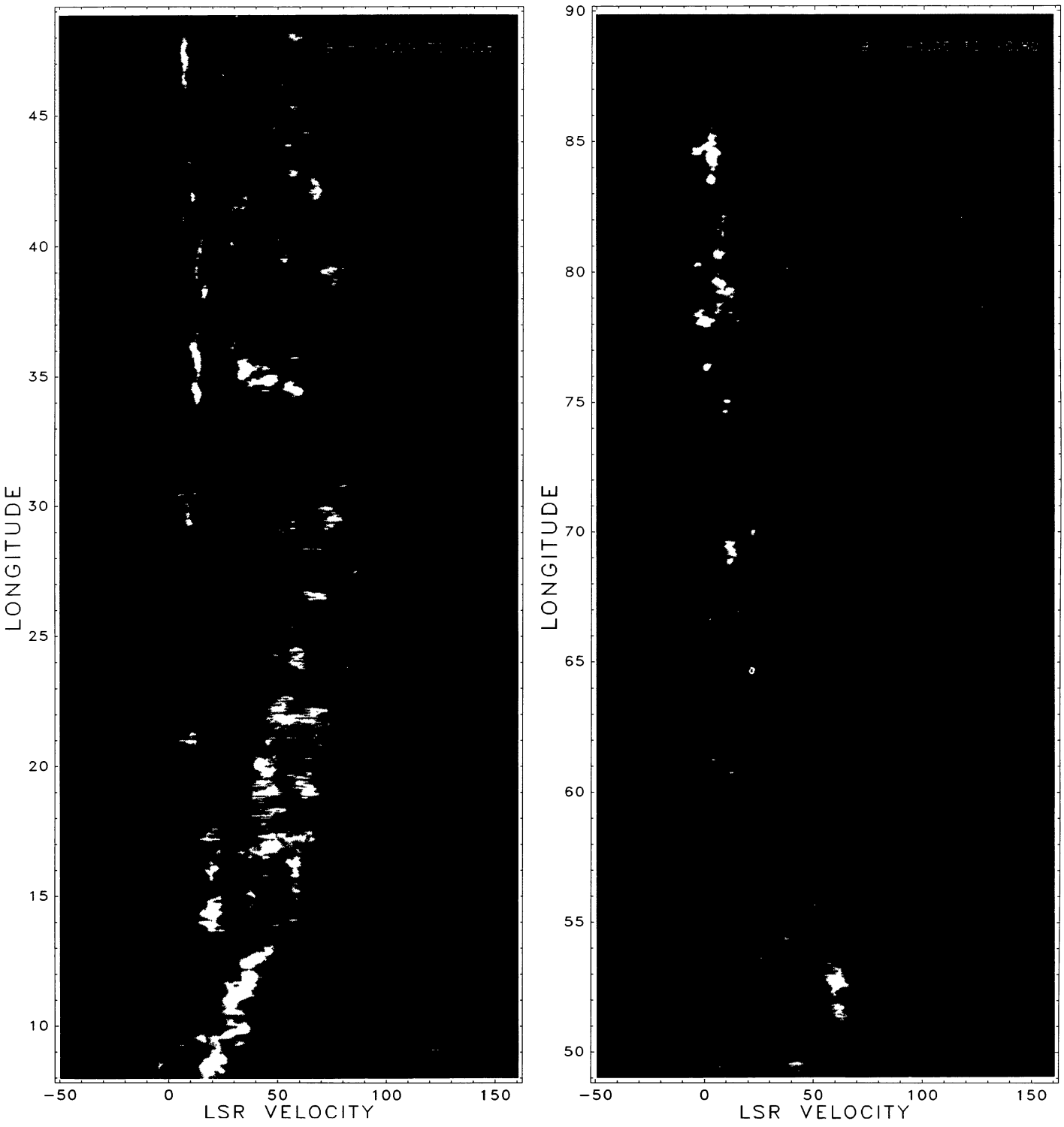

FIG. 1*g*

CLEMENS, SANDERS, SCOVILLE, AND SOLOMON (*see* page 298)

PLATE 8

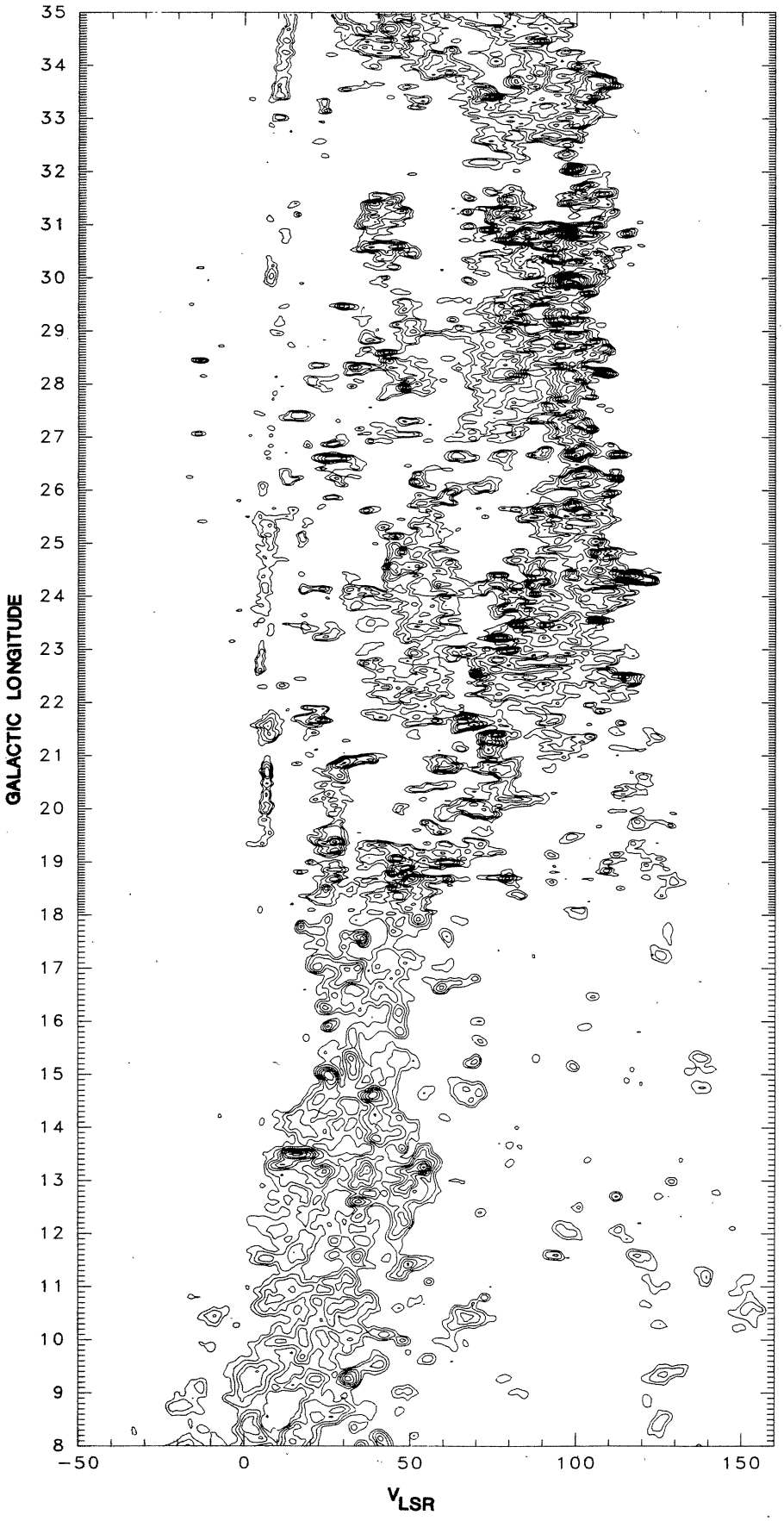

FIG. 2*a*

FIG. 2.—Longitude-velocity (l, V) diagram for $b = 0°$ data only in contoured format. Longitude sampling is indicated by tick marks along the vertical axes. Velocity resolution is 1 km s^{-1}. The lowest contour is at 1.25 K (3 σ), and subsequent contours are at integer temperatures (2,3,4,...). Note how many of the smooth-looking features in Fig. 1 break up into individual molecular clouds. (*a*) From $l = 8°$ to $l = 35°$. (*b*) From $l = 35°$ to $l = 62°$. (*c*) From $l = 62°$ to $l = 90°$.

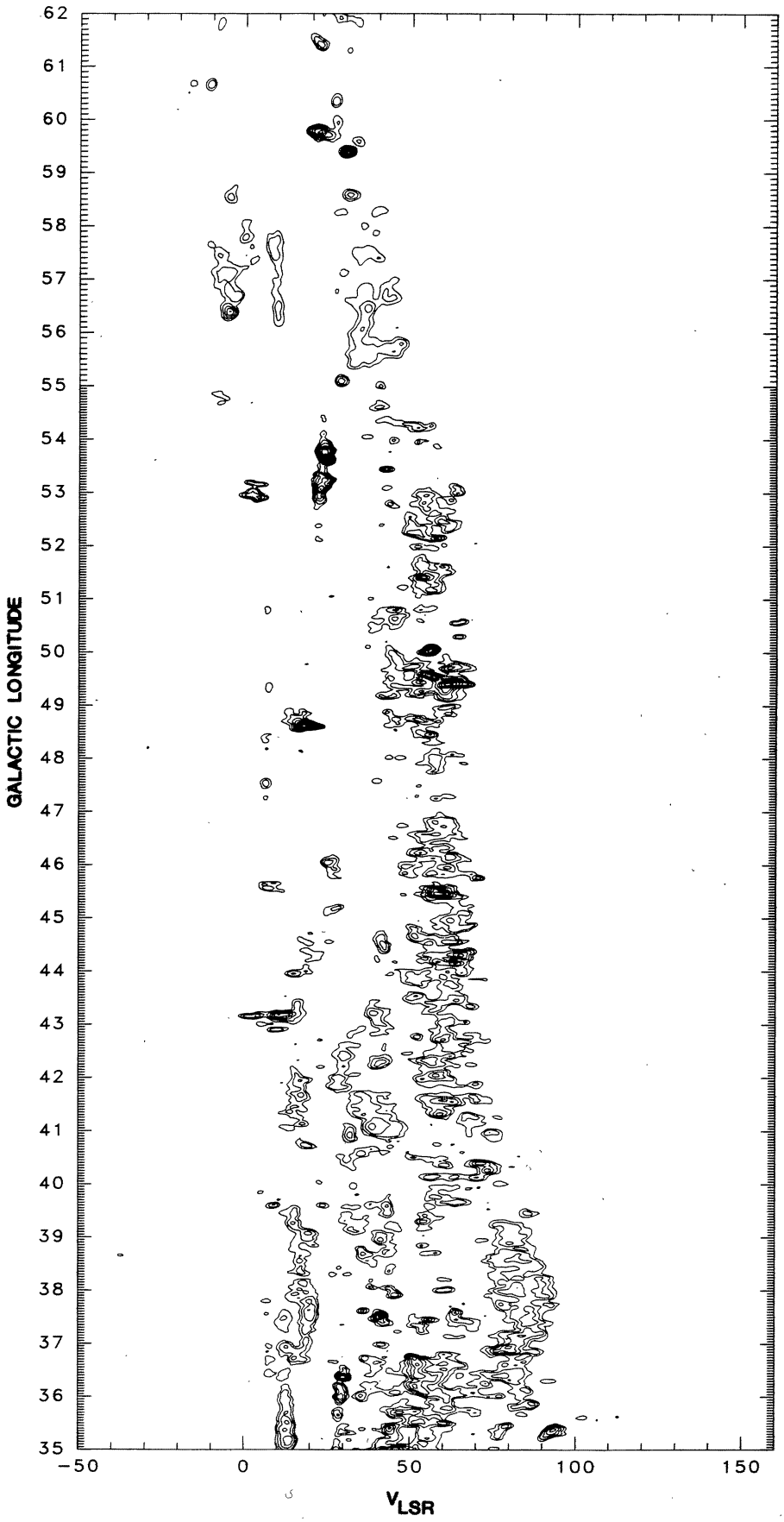

FIG. 2*b*

PLATE 10

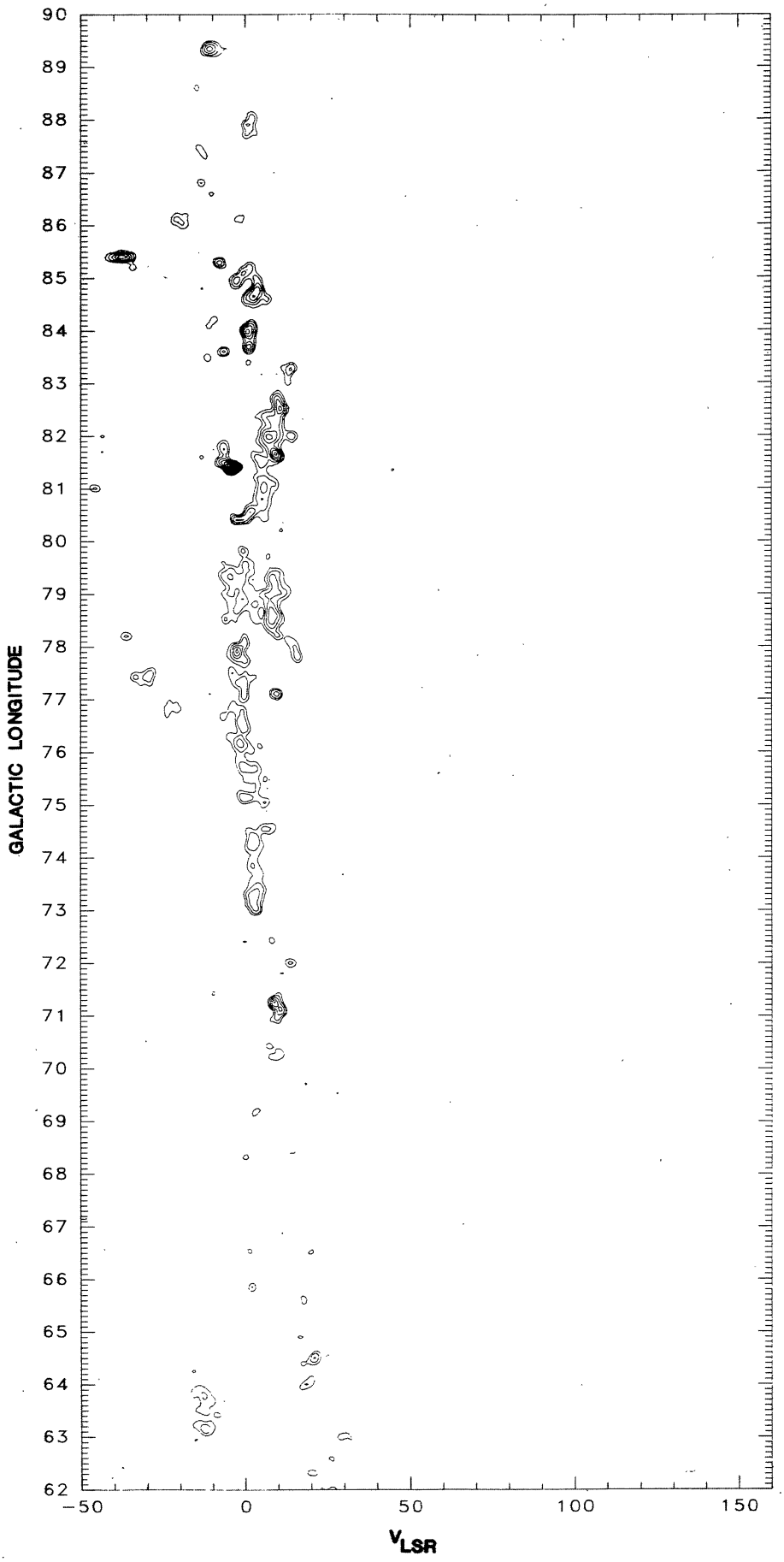

FIG. 2*c*

CLEMENS, SANDERS, SCOVILLE, AND SOLOMON (*see* page 298)

1986ApJS...60..297C

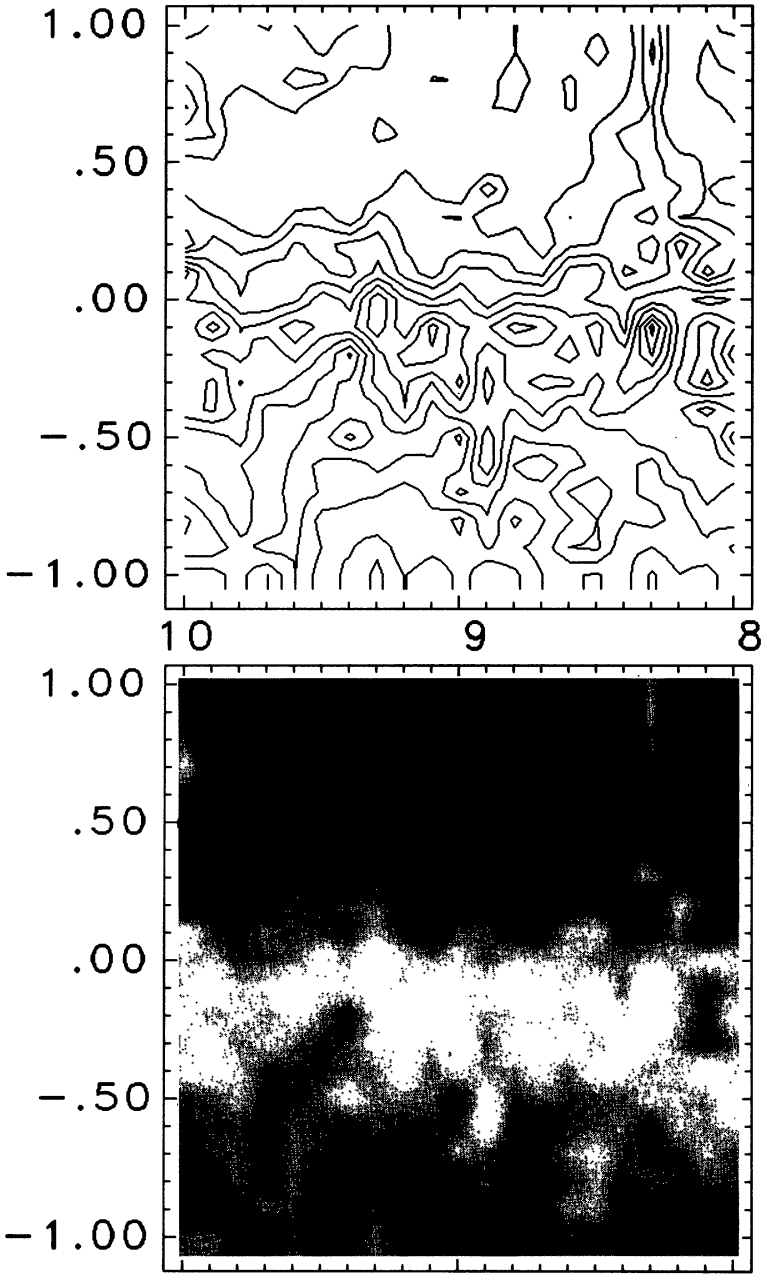

MASSACHUSETTS–
STONY BROOK
GALACTIC PLANE
CO SURVEY

$$\int_{-50}^{+160} T_{CO}\, dV$$

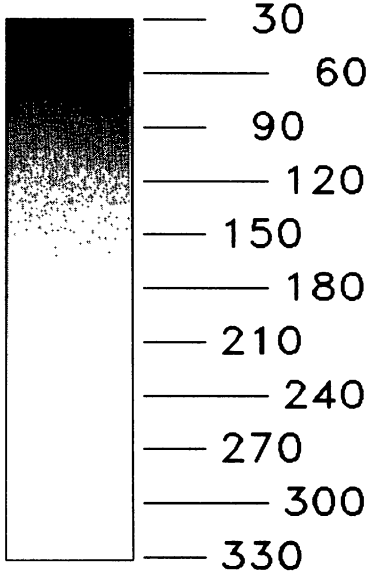

FIG. 4.—*Upper panel*: Contour map of integrated CO intensity versus Galactic longitude (*horizontal axis*) and latitude (*vertical axis*) for $l = 8°–10°$ and for $b = -1°.05$ to $+1°.00$. The lowest contour is at 30 K km s^{-1} (3 σ) and subsequent contours are stepped by 30 K km s^{-1}. *Lower panel*: Gray scale representation of map in upper panel. Gray scale "wedge" shows correspondence between gray level and integrated intensity.

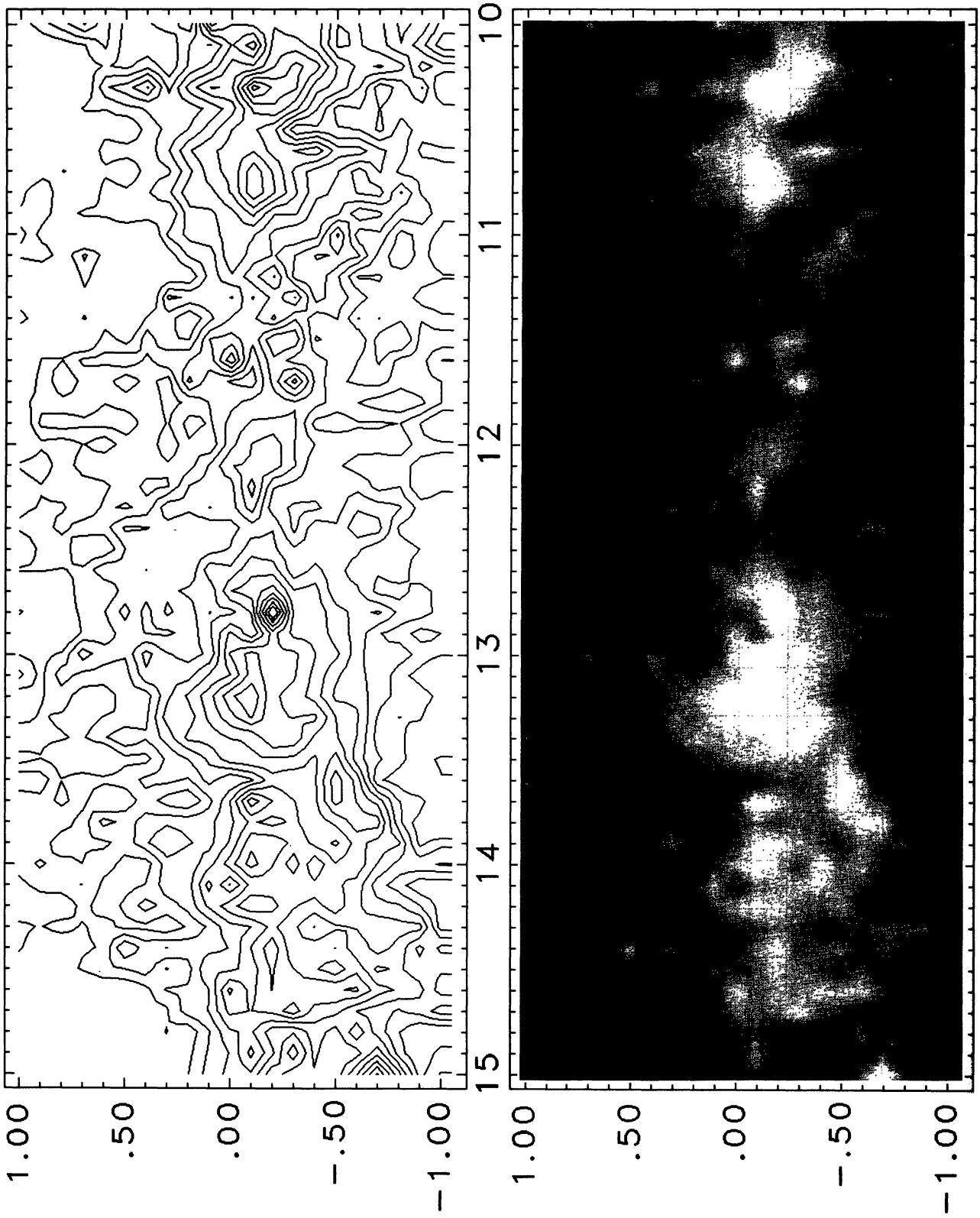

FIG. 5.—Same as Fig. 4, but for $l = 10°$–$15°$.

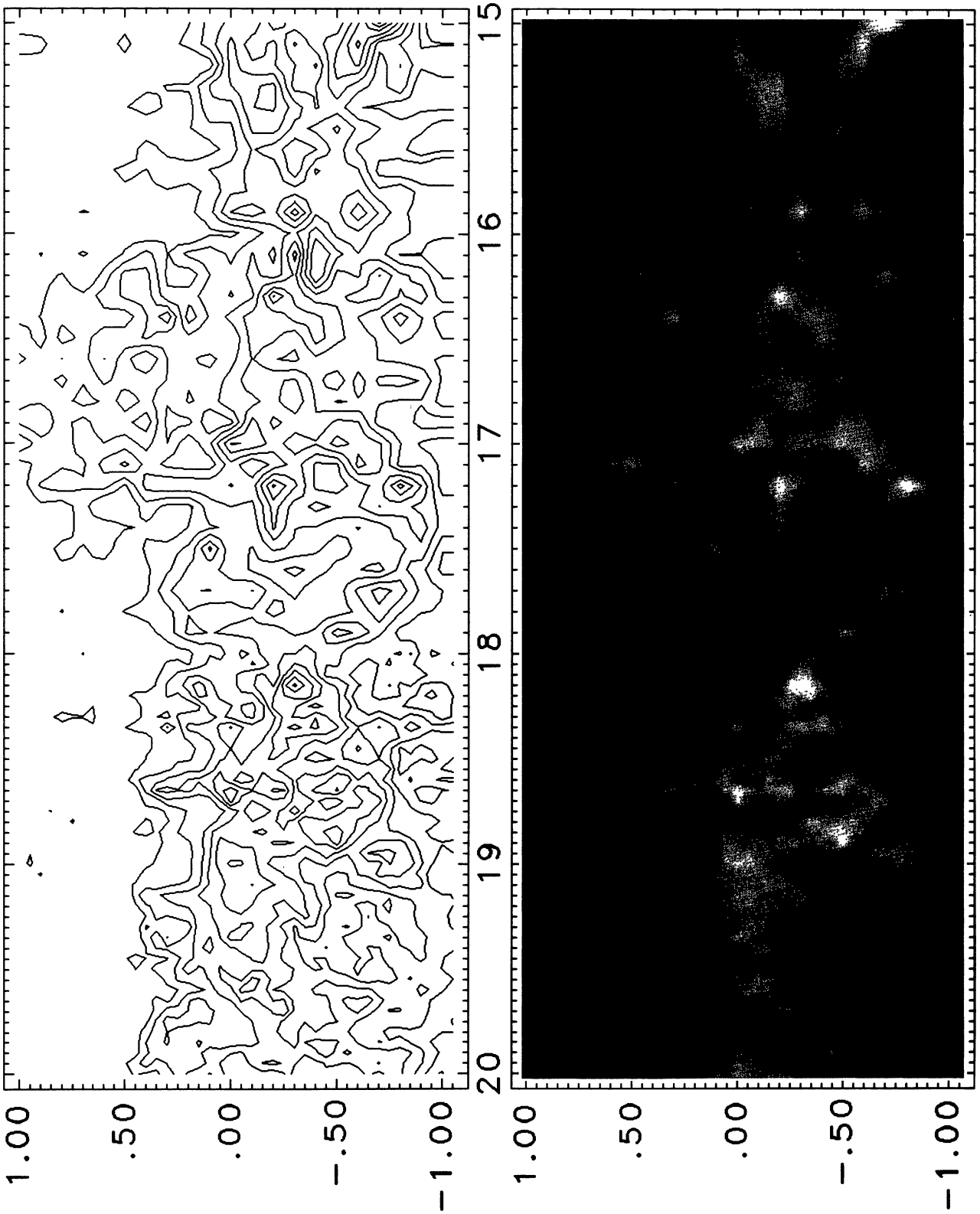

FIG. 6.—Same as Fig. 4, but for $l = 15°$–$20°$. Note resolution change at $l = 18°$.

PLATE 14

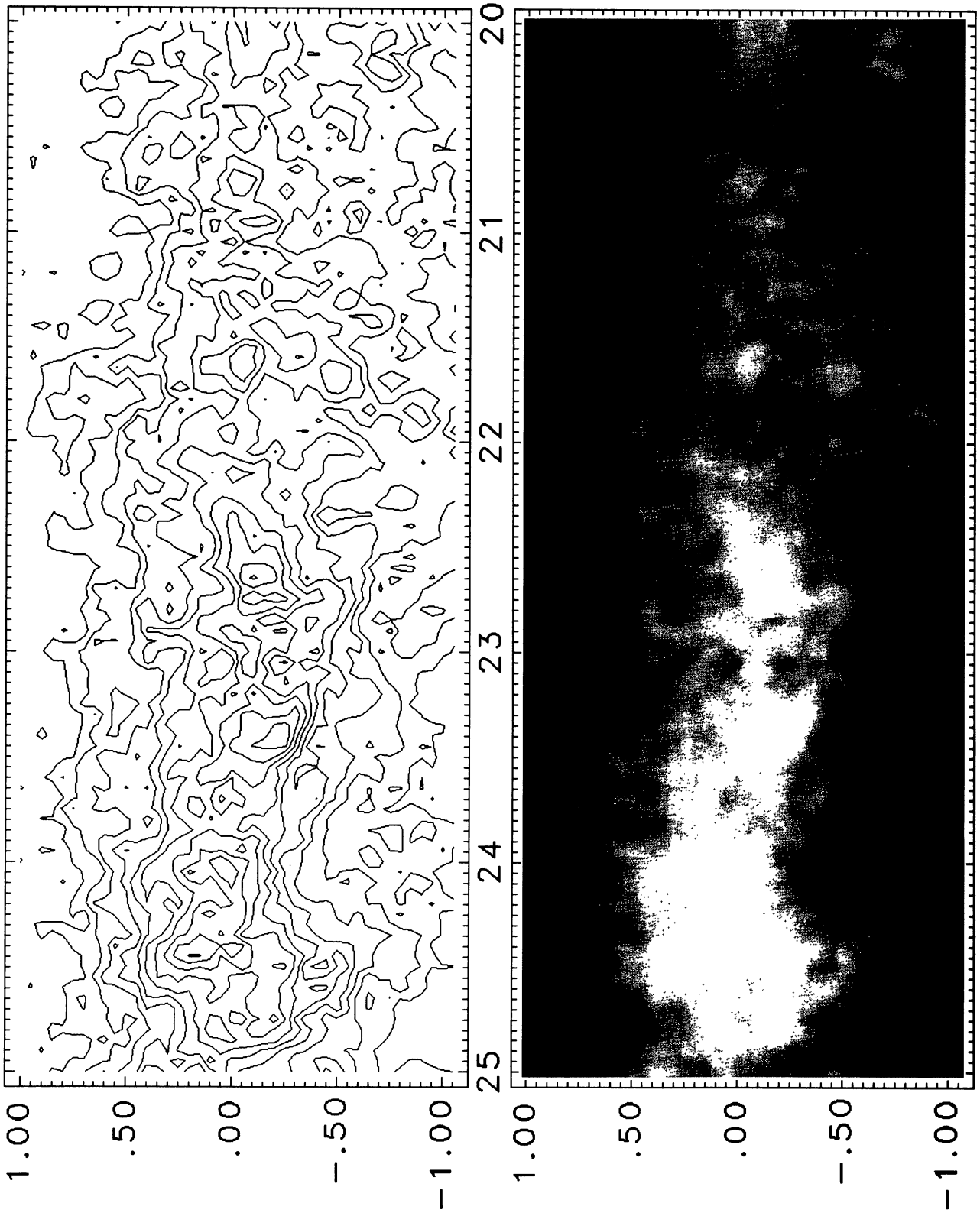

FIG. 7.—Same as Fig. 4, but for $l = 20°–25°$.

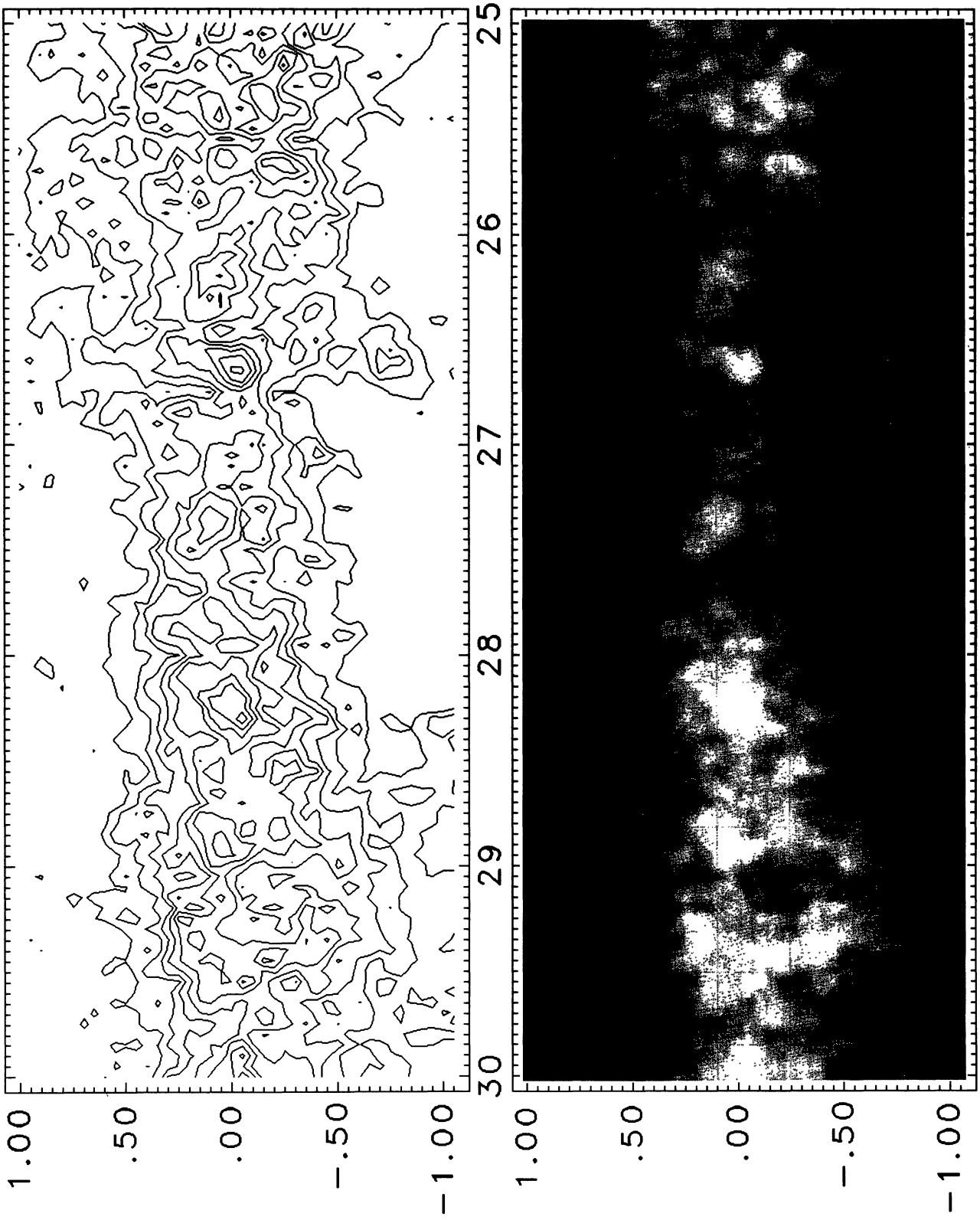

FIG. 8.—Same as Fig. 4, but for $l = 25°-30°$.

PLATE 16

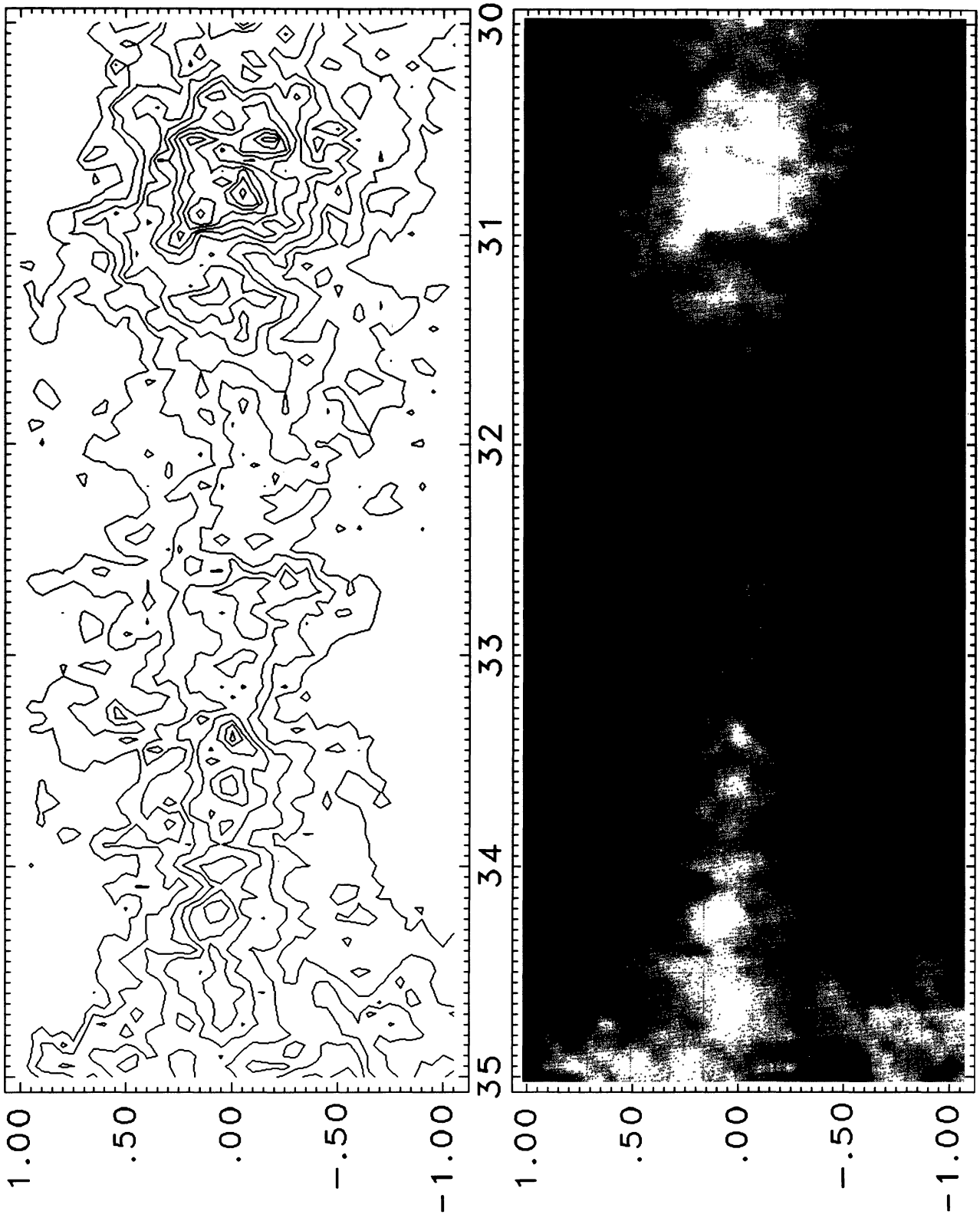

FIG. 9.—Same as Fig. 4, but for $l = 30°–35°$.

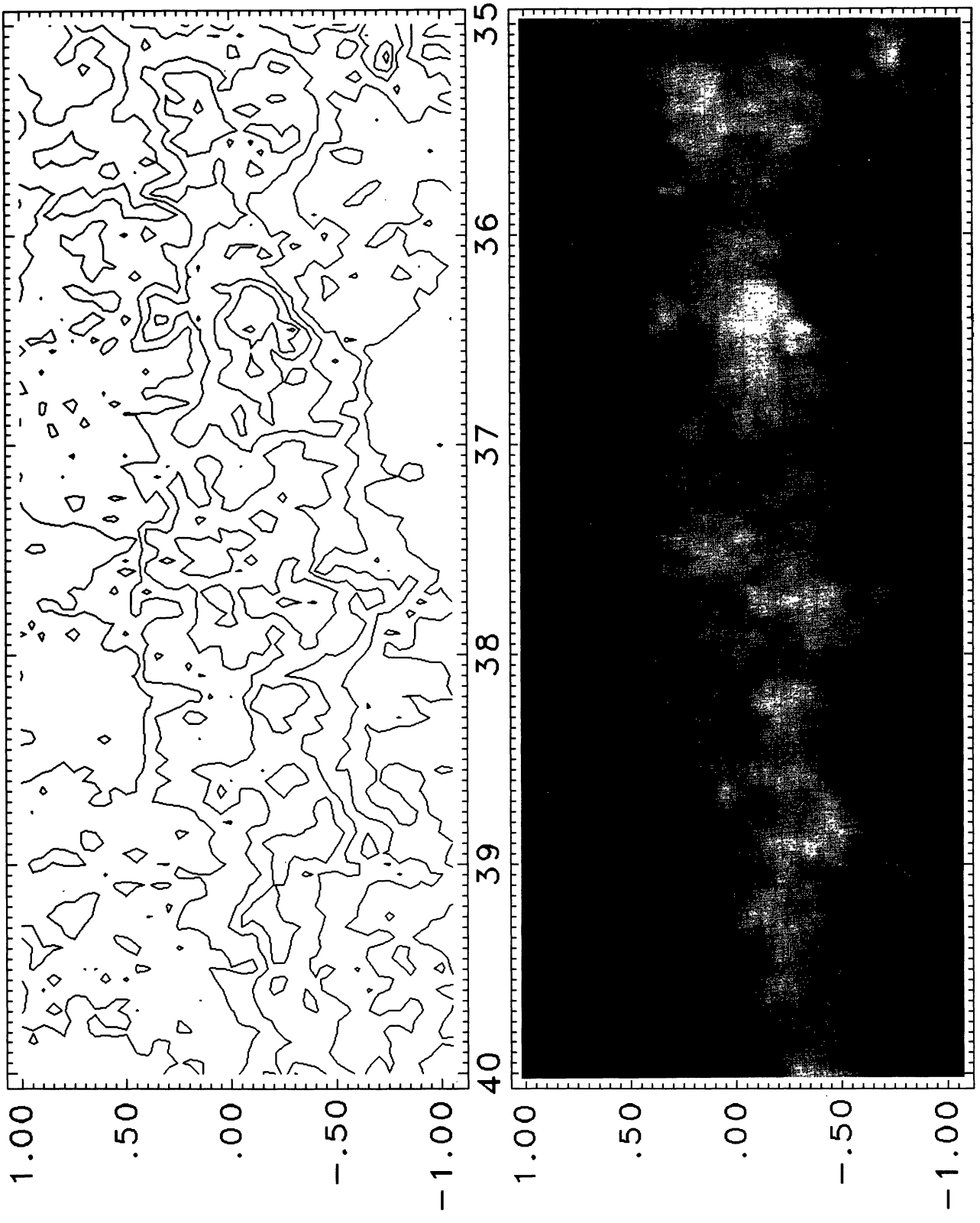

FIG. 10.—Same as Fig. 4, but for $l = 35°$–$40°$.

PLATE 18

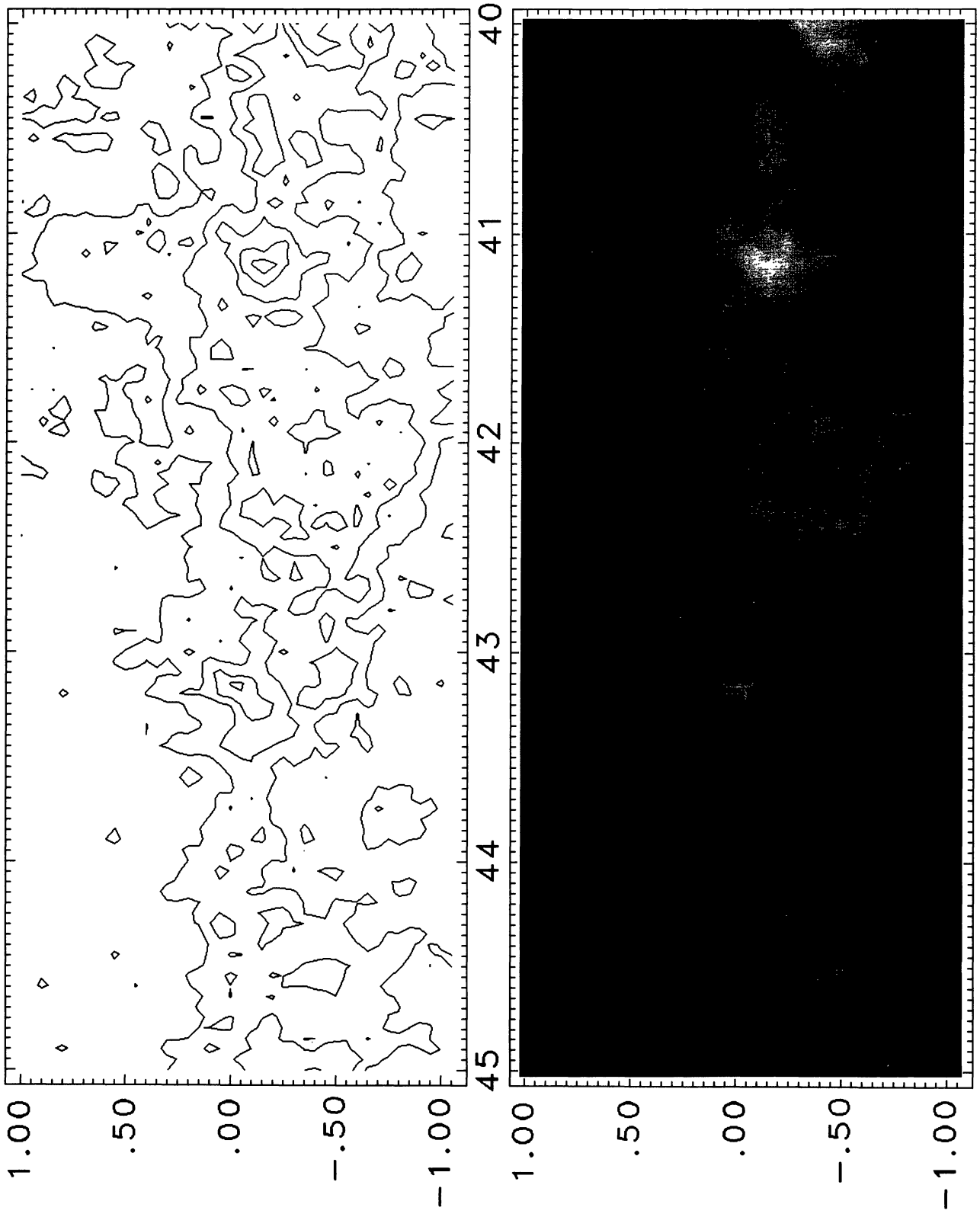

FIG. 11.—Same as Fig. 4, but for $l = 40°$–$45°$.

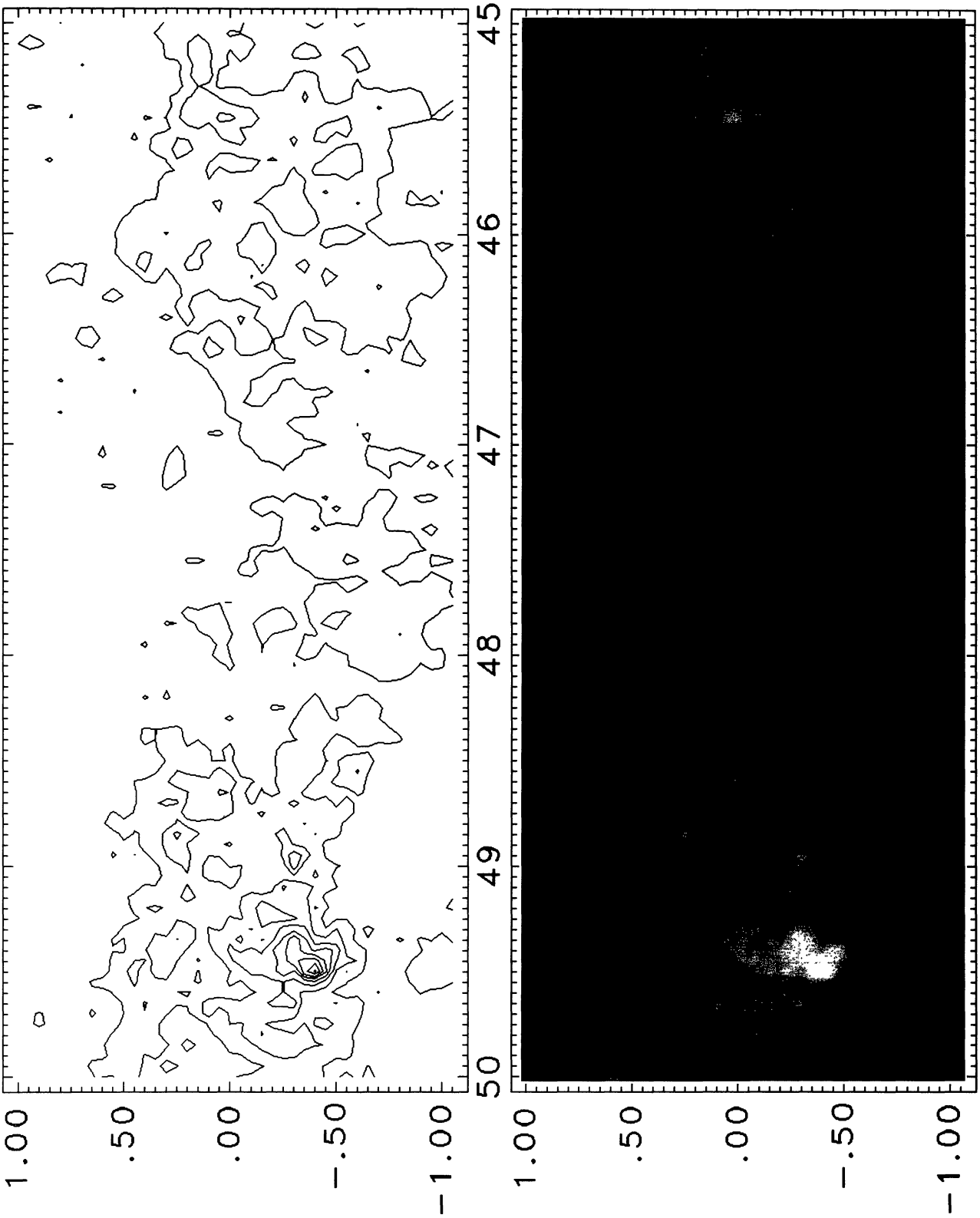

FIG. 12.—Same as Fig. 4, but for $l = 45°$–$50°$.

PLATE 20

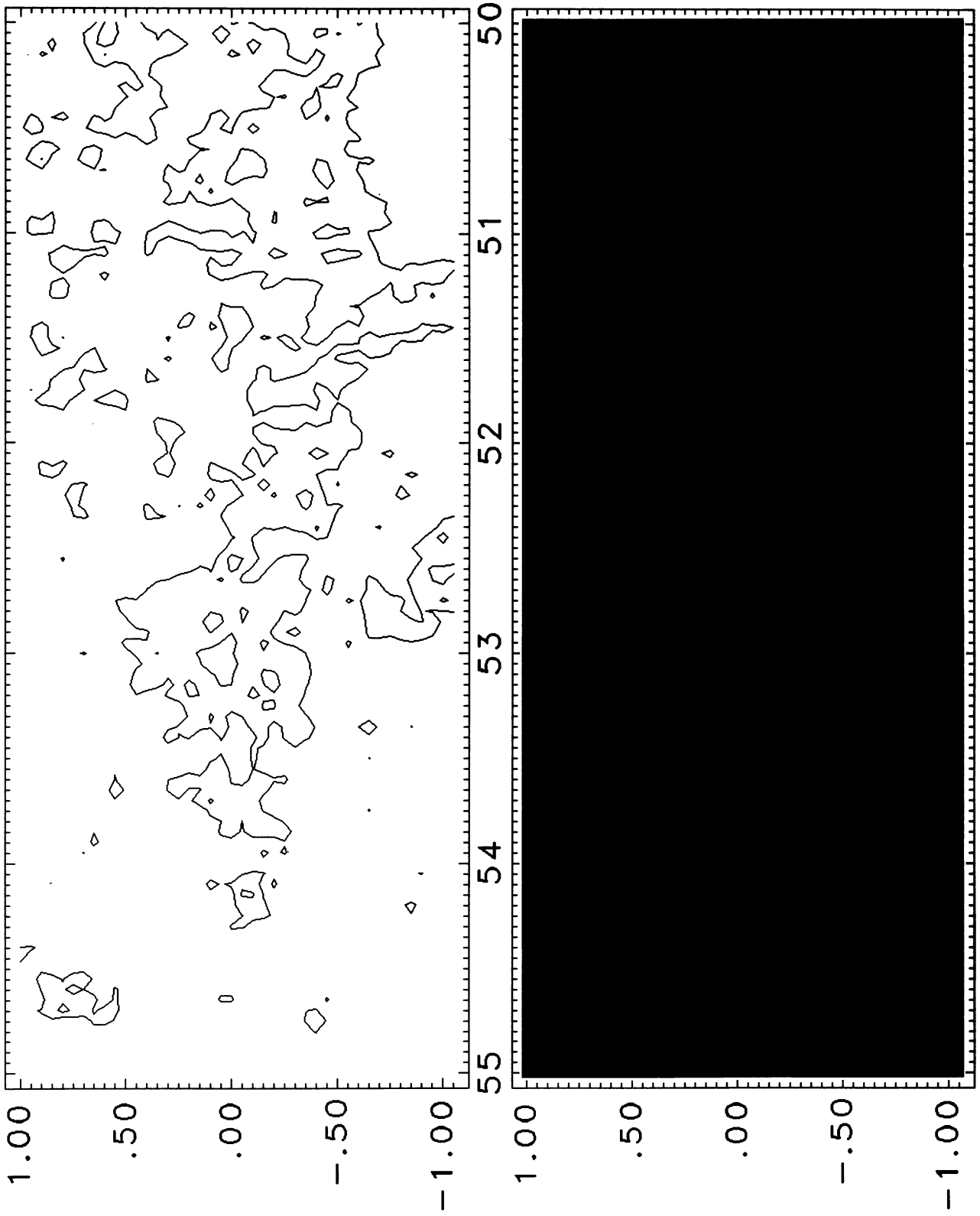

FIG. 13.—Same as Fig. 4, but for $l = 50°$–$55°$.

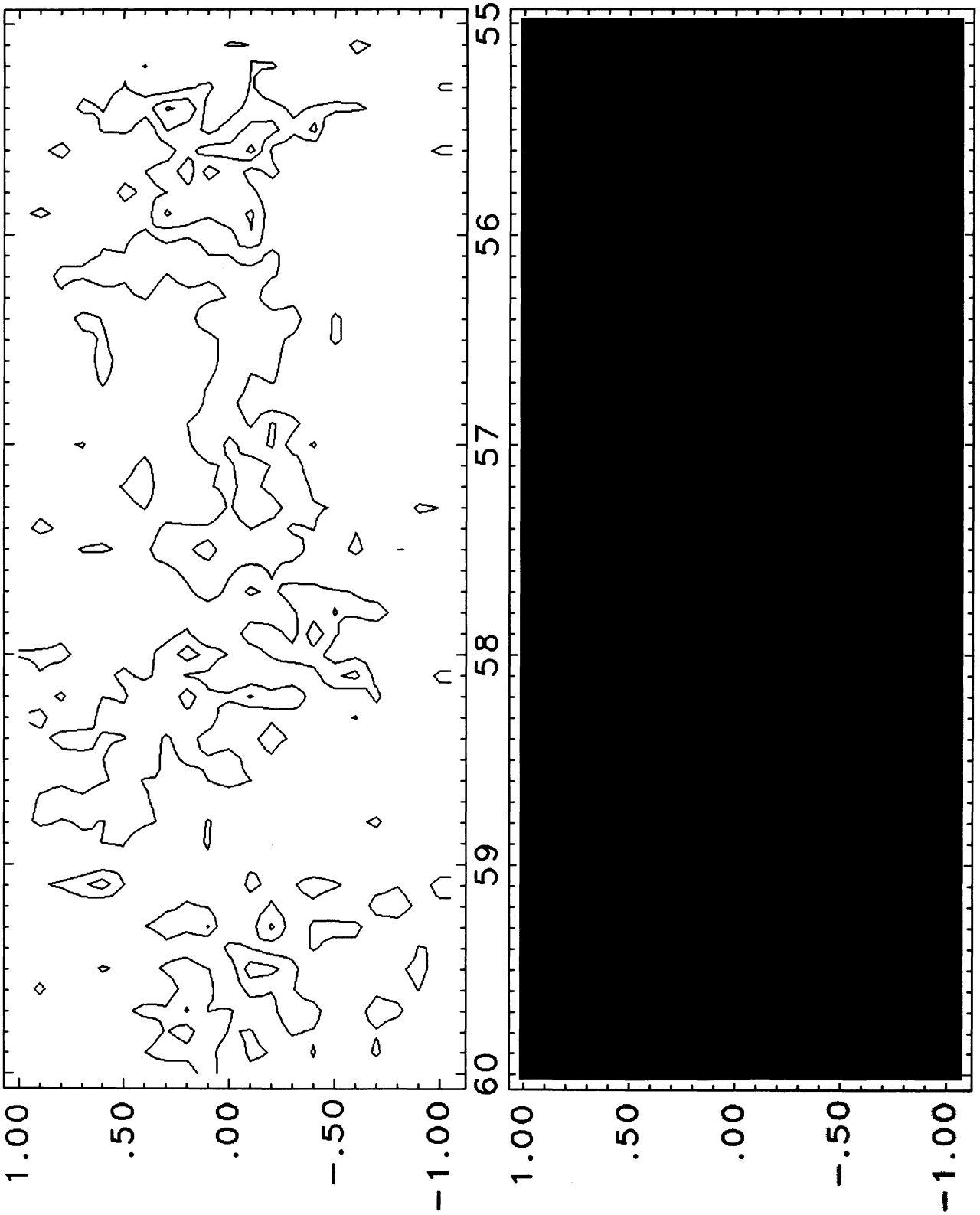

FIG. 14.—Same as Fig. 4, but for $l = 55°–60°$.

PLATE 22

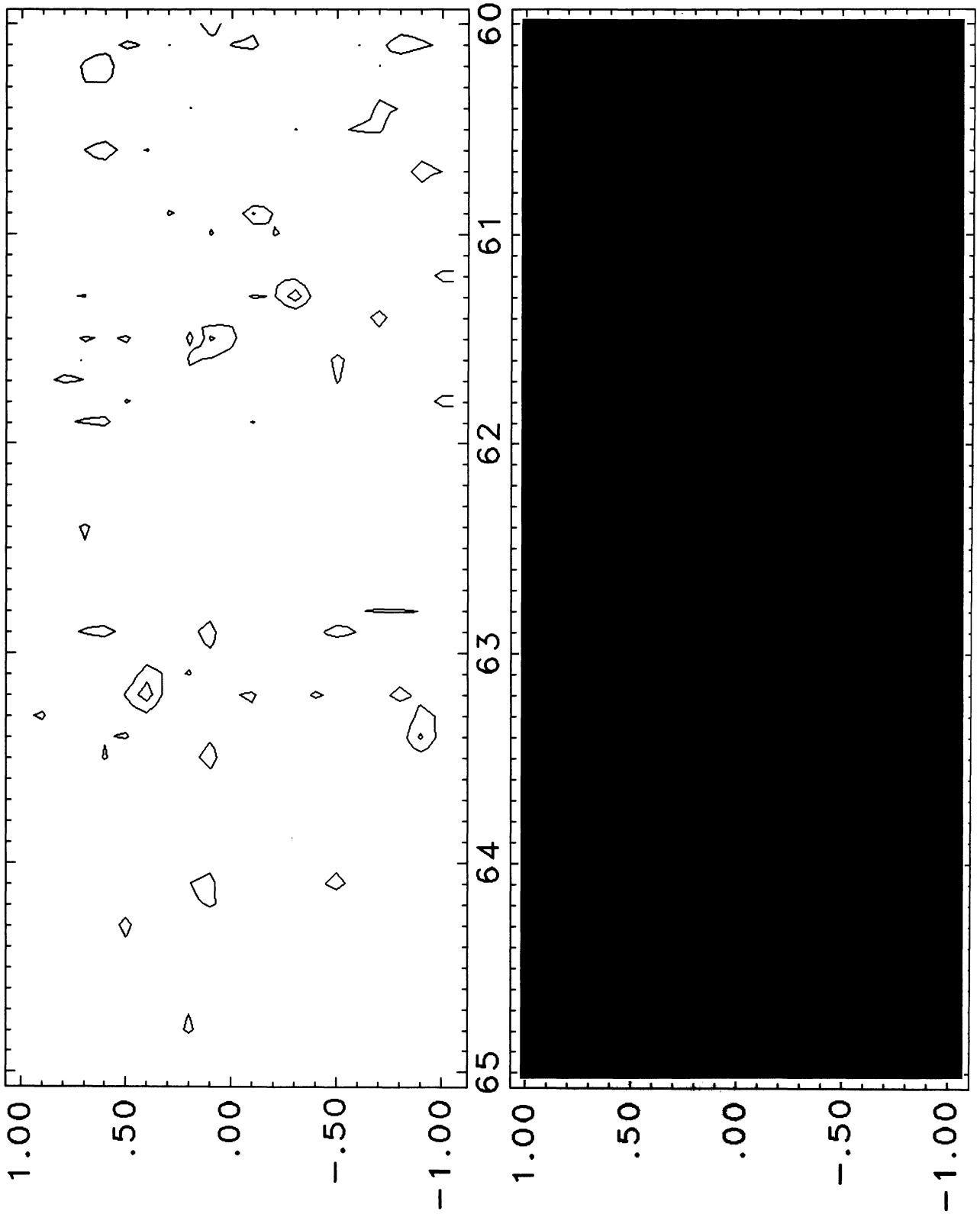

FIG. 15.—Same as Fig. 4, but for $l = 60°$–$65°$.

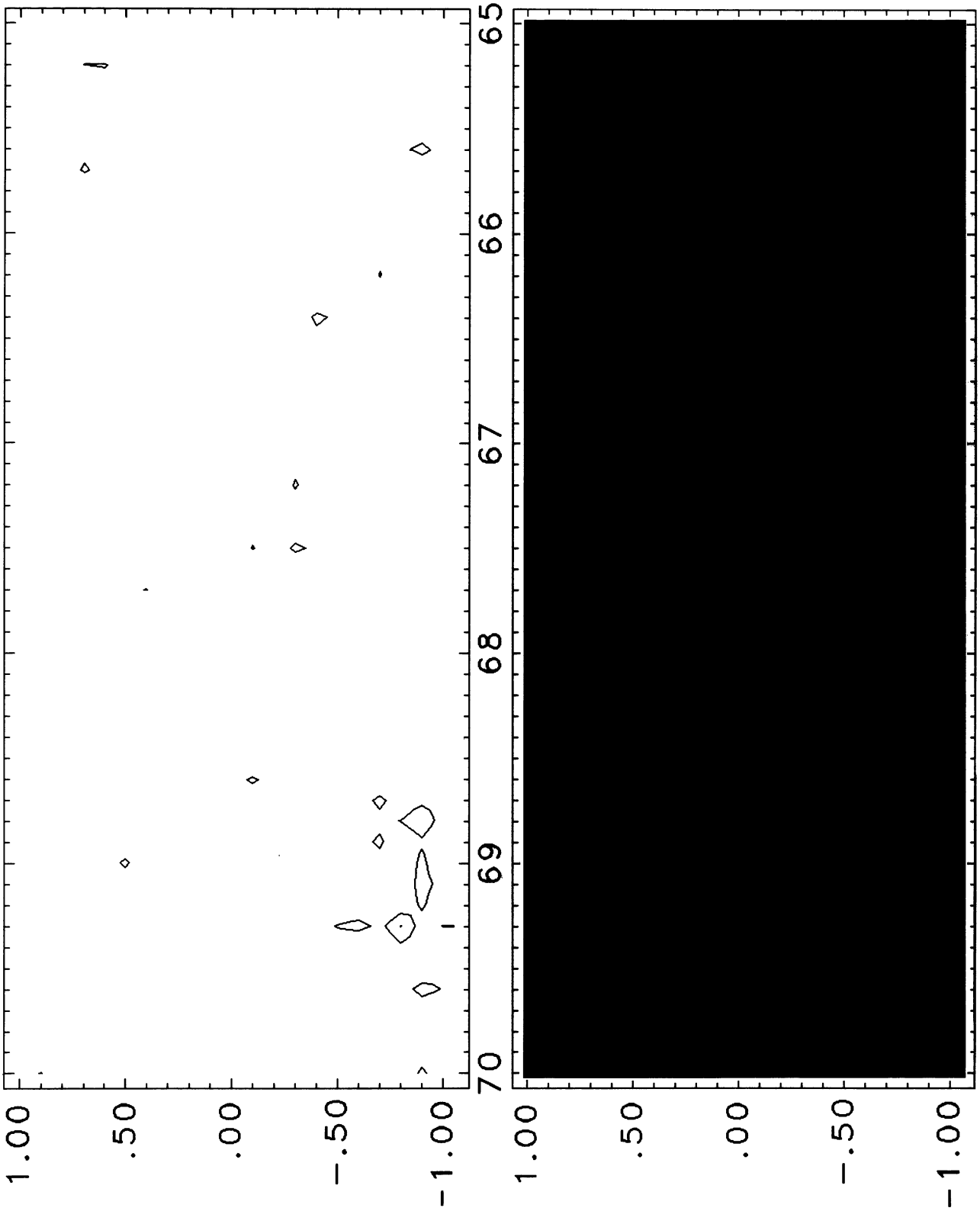

FIG. 16.—Same as Fig. 4, but for $l = 65°-70°$.

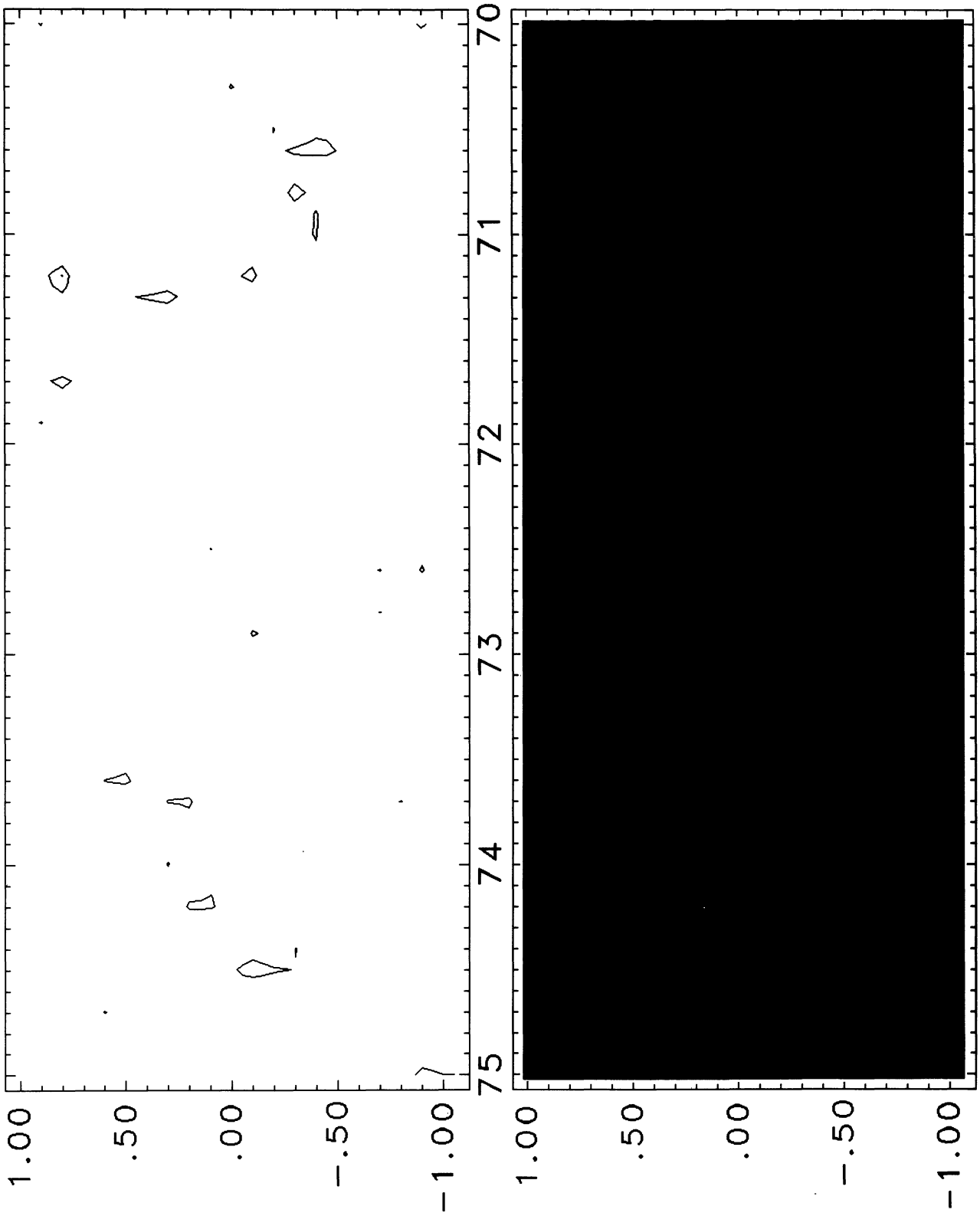

FIG. 17.—Same as Fig. 4, but for $l = 70°–75°$.

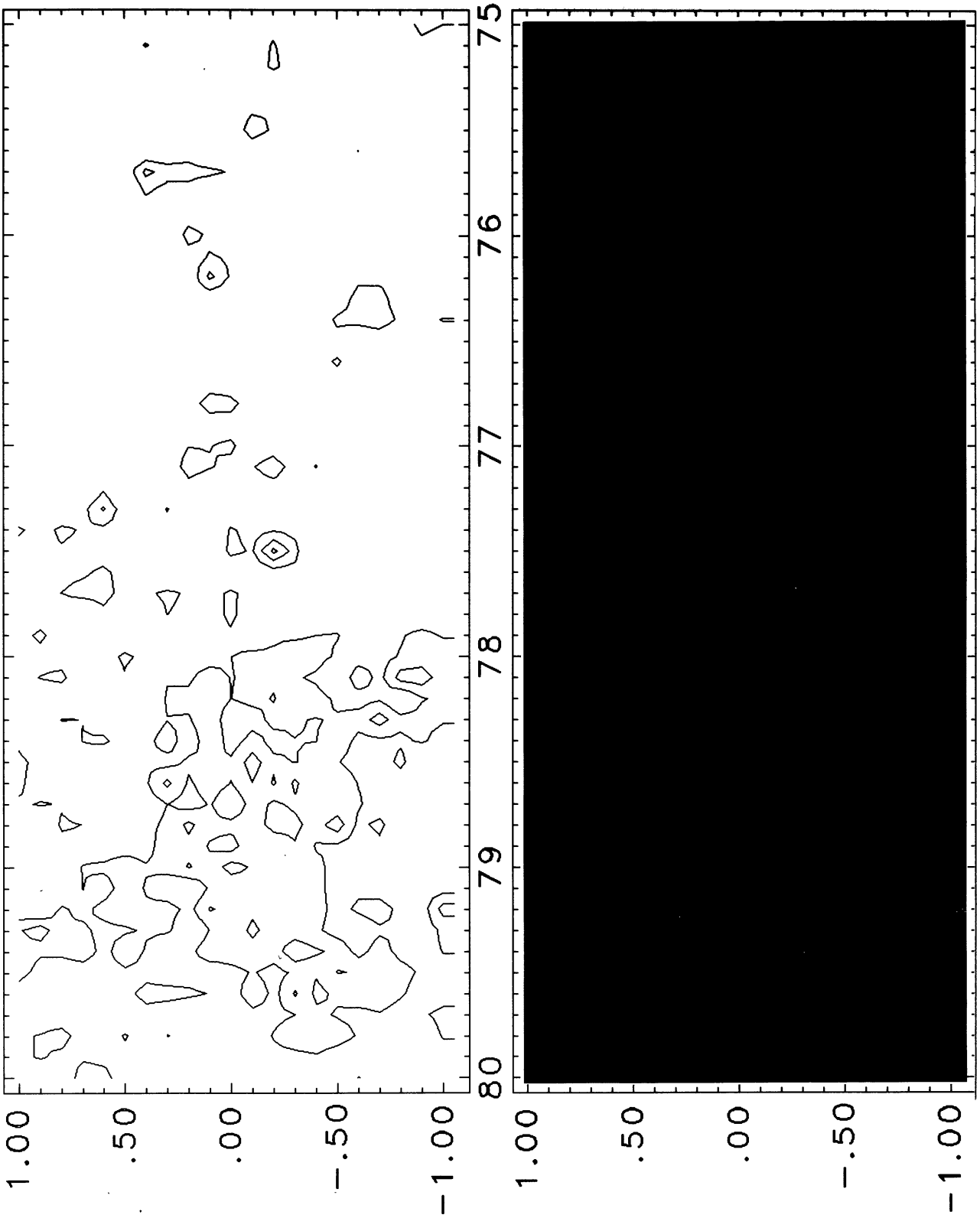

FIG. 18.—Same as Fig. 4, but for $l = 75°–80°$.

PLATE 26

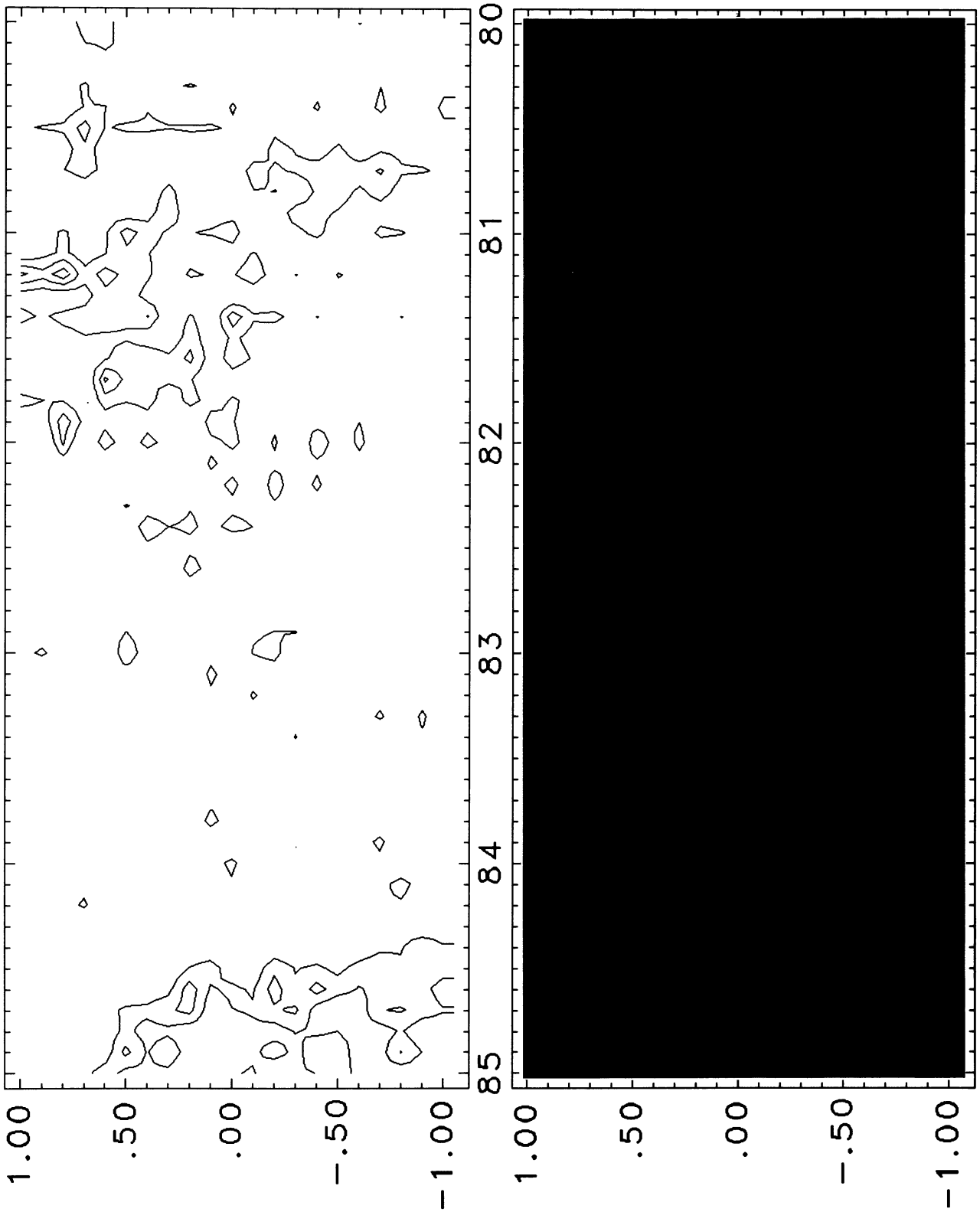

FIG. 19.—Same as Fig. 4, but for $l = 80°$–$85°$.

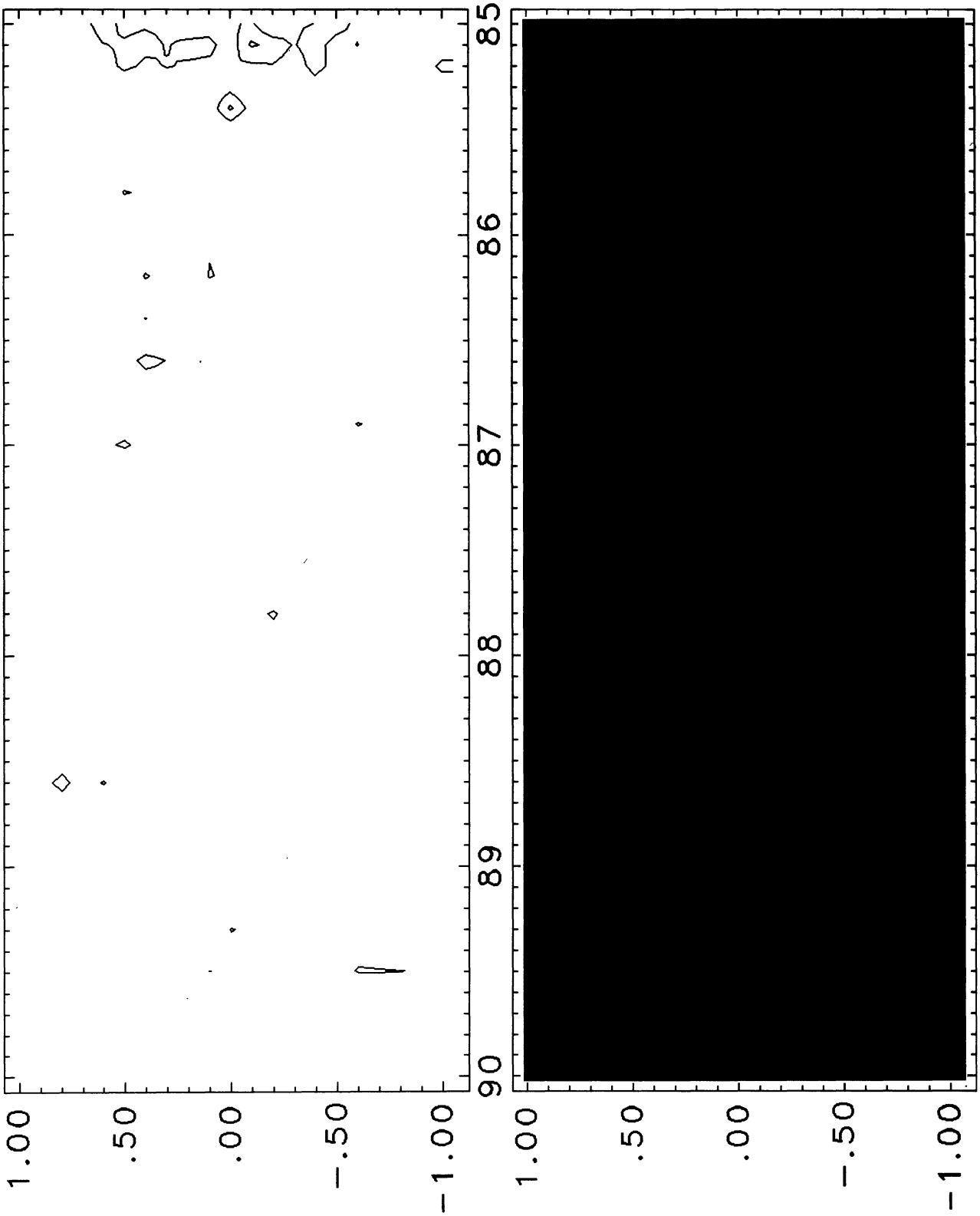

FIG. 20.—Same as Fig. 4, but for $l = 85°-90°$.